

# Improved Rate-Energy Trade-off For SWIPT Using Chordal Distance Decomposition In Interference Alignment Networks

Navneet Garg<sup>1</sup>, Avinash Rudraksh, Govind Sharma, Tharmalingam Ratnarajah

**Abstract**—This paper investigates the simultaneous wireless information and power transfer (SWIPT) precoding scheme for K-user multiple-input-multiple-output (MIMO) interference channels (IC), for which interference alignment (IA) schemes provide optimal precoders to achieve full degrees-of-freedom (DoF) gain. However, harvesting RF energy simultaneously reduces the achievable DoFs. To study a trade-off between harvested energy and sum rate, the transceiver design problem is suboptimally formulated in literature via convex relaxations, which is still computationally intensive, especially for battery limited nodes running on harvested energy. In this paper, we propose a systematic method using chordal distance (CD) decomposition to obtain the balanced precoding, which improves the trade-off. Analysis shows that given the nonnegative value of CD, the achieved harvested energy for the proposed precoder is higher than that for perfect IA precoder. Moreover, energy constraints can be achieved, while maintaining a constant rate loss without losing DoFs via tuning the CD value and splitting factor. Simulation results verify the analysis and add that the IA schemes based on max-SINR or mean-squared error are better suited for SWIPT maximization than subspace or leakage minimization methods.

**Index Terms**—Chordal distance; interference alignment; power splitting; rate-energy trade-off; Simultaneous wireless information and power transfer (SWIPT).

## I. INTRODUCTION

In wireless networks, energy consumption is one of the major issues due to increasing number of devices and the need for environment protection [1]. Green communications have attracted much interest from academia and industry. In the past few years, wireless energy harvesting (EH) has emerged as an important method to achieve green wireless communications [2]. In EH, the energy collected from the ambient environment can be utilized as a power supply for self-sustained wireless nodes [3], [4]. Since radio frequency (RF) signals carry energy, these signals can act as a new source for EH. Wireless power transfer (WPT) is becoming an important segment in future wireless communications. The experiment results in [5] demonstrate that a few microwatts of RF power is harvested from the broadcast signals of TV stations, which are located at several kms away. Therefore, wireless EH system can be used for energy-constrained devices, smart wearables, and implantable sensors [6]. On the

other hand, since RF signals also communicate information in wireless systems, simultaneous information and power transfer (SWIPT) technology have attracted great research interests [7]–[12]. Some pioneering works on SWIPT have been done in [13], [14], where the rate-energy region has been characterized for single antenna point-to-point system. In [15], for multiple-input-multiple-output (MIMO) broadcast network, dedicated EH and information decoding (ID) receivers are used. The time switching duration (in time-division access) or power splitting (PS) ratio (in frequency-division access) is computed using iterative convexified algorithm in [16]. [17] proposes the quantized CSI feedback to improve EH, and derives the trade-off between EH duration and ID.

Further, for interference channels (ICs), interference is one of the most fundamental and challenging aspects. Regarding interference cancellation, from the last decade, interference alignment (IA) has emerged as a promising solution for MIMO wireless networks. Under certain conditions, IA has been shown to be degree of freedom (DoF) optimal for ICs [18]. In IA, the precoders at the sources and the decoders at the destinations are employed to align and cancel the interfering signal from other users [18]. To design these IA precoders and decoders, several iterative algorithms have been investigated in the literature, such as signal-to-interference-plus-noise-ratio (SINR) maximization, leakage minimization [19], [20], mean squared error (MSE) minimization [21], [22], alternating minimization [23], etc. These IA algorithms assume channel state information (CSI) available at the sources to compute the IA precoders. In frequency division duplexed (FDD) systems, this information is obtained at the sources using CSI feedback either in quantized or in analog form [24]–[28]. In quantized CSI feedback, the linear rate scaling is maintained at a given signal-to-noise-ratio (SNR), only if the number of bits are scaled proportional to SNR [27], [29]–[31]. For analog feedback, a constant rate-loss has been observed at medium-to-high SNR regime, i.e., without any loss of DoFs.

Next, for IA networks, the interference component is canceled at each receiver to separate out the desired signal. However, before interference nulling, the received signal can be split, and the interference power can be utilized for harvesting energy. A review of SWIPT schemes is given as follows. In [32] with 2-users IC, different possible transmission strategies are defined for time-switching (TS) receivers. Authors in [33] collaboratively obtain the optimal TS duration for 2-user IC, which is further extended to  $K$ -users via introducing user-groups. In [34] for multiple-input-single-output (MISO) IC, PS

N. Garg and T. Ratnarajah are with The University of Edinburgh, UK. A. Rudraksha and G. Sharma are with Indian Institute of Technology Kanpur, India. E-mails: {ngarg@ed.ac.uk, avinash.rudraksha@gmail.com, govind@iitk.ac.in, t.ratnarajah@ed.ac.uk}. This work was supported by the UK Engineering and Physical Sciences Research Council (EPSRC) under grant number EP/P009549/1.

ratio and power allocation is obtained to show that maximal ratio transmission (MRT) based precoding outperforms zero-forcing (ZF) in terms of EH. The work in [35] is to improve harvested energy and its consumption problem via power allocation, while keeping fairness among users. In [36], [37], antenna selection is used for EH improvements. In [38], an upper bound on EH is derived. In [11], [39], semi-definite relaxation technique is leveraged to obtain suboptimal solutions via convexifying the joint transceiver design problem. In [1], power splitting algorithm is proposed to maximize a linear-sum of rate and energy objectives, where the coefficient of the linear-sum decides the weight of these objectives.

### A. Contributions

In this paper, a systematic precoding approach for SWIPT maximization is investigated for the  $K$ -user MIMO-IC. From the above review, it can be noted that in IA-SWIPT literature, authors have posed the optimization problem as a linear sum of sum rate and harvested energy, and sub-optimum solution have been computed convex relaxation tools [11], [39]. In this work, using chordal distance (CD) decomposition, a systematic method is presented to obtain the balanced precoding, which improves the trade-off between sum rate and harvested energy. The proposed precoder, which is the key for the rate-energy trade-off, can be obtained via maximizing the harvested energy, or sum rate via tuning the value of chordal distance. EH analysis shows the guaranteed improvement of energy for the proposed formulation. Simulation results for different IA methods have been compared. These results show that the IA methods utilizing direct channels, such as MMSE and max-SINR algorithms, provide the better harvested power than that of the IA methods, which does not utilize direct channels in the precoder design including subspace method or leakage minimization algorithm. Analog feedback automatically chooses the chordal distance, which provides better EH and linear sum rate scaling at high SNR. On the other hand, with quantized feedback, increasing the size of codebook increases harvested energy, while suffering DoF losses. In summary, the contribution of this paper can be listed as follows:

1) *Rate energy balanced precoding*: First, the maximum harvested energy achievable is obtained using the precoders  $\mathbf{V}^{EH}$ , which defines the upper limit achievable on EH. Then, we systematically derive the balanced precoding scheme to improve SWIPT trade-off using CD decomposition. Beyond the upper limit i.e., when the CD value between IA and the proposed precoder is chosen greater than the CD value between the IA precoder and  $\mathbf{V}^{EH}$ , the precoder  $\mathbf{V}^{EH}$  provides the better sum rates. It is also worth noting that the proposed method is much computationally efficient, as compared to semi-definite programming.

2) *Simple parameter design for constant rate loss*: We analyze the upper and lower bounds on the harvested energy. Tuning the values of CD and PS ratio, the trade-off between sum rate and harvested energy for IA networks can be observed. Further, the cases of analog and quantized feedback are analyzed, where the CD value is automatically set based on the feedback transmission power in the analog feedback,

and based on the size of codebook in the quantized feedback. In both cases, harvested energy is shown to improve than that in the case of IA precoder. Moreover, it is shown that it is possible to obtain constant rate loss (i.e., linear sum rate scaling with respect to SNR), while achieving the desired harvested energy threshold.

3) *Which is the best IA scheme for harvesting?*: Simulation results verify the improvements and limits of balanced precoder via the plots for rate-energy regions, and show that MSE based IA schemes are better suited for SWIPT trade-offs than subspace or leakage minimization schemes. Both analog and quantized feedback improves the harvested energy, while achieving a constant rate loss in the former case, and getting the rate loss proportional to the chordal distance in the latter case.

*Organization*: The interference channel model is given in section II. The next sections III and IV present energy optimized precoding and the proposed balanced precoding, followed by the cases of analog and quantized feedback in section V. Simulation results are presented in Section VI. Section VII concludes the work.

*Notations*: Scalars, vectors and matrices are represented by the lower case ( $a$ ), lower case bold face ( $\mathbf{a}$ ) and upper case bold face ( $\mathbf{A}$ ) letters respectively. Conjugate, transpose, Hermitian transpose and Kronecker product of matrices are denoted by  $(\cdot)^*$ ,  $(\cdot)^T$ ,  $(\cdot)^\dagger$  and  $\otimes$  respectively.  $\mathcal{CN}(\mu, \mathbf{R})$  represents a circularly symmetric complex Gaussian random vector with mean  $\mu$  and covariance matrix  $\mathbf{R}$ . The notations  $\|\cdot\|$  and  $\|\cdot\|_F$  denote the  $l_2$  norm and Frobenious norm.  $\text{vec}(\mathbf{X})$  denotes the column-wise vector representation of matrix  $\mathbf{X}$ .  $\mathcal{D}(\mathbf{A}_i)$  denotes a block diagonal matrix with matrices  $\mathbf{A}_i$  as its block diagonal components.  $\mathcal{O}(\mathbf{X})$  denotes the orthonormal part of the QR decomposition of  $\mathbf{X}$  [21].  $\mathbf{X}$  is unitary means  $\mathbf{X}\mathbf{X}^\dagger = \mathbf{X}^\dagger\mathbf{X} = \mathbf{I}$ .  $\lambda_{\max}(\mathbf{A})$ ,  $\nu_{\max}(\mathbf{A})$ ,  $\nu_{1:d}(\mathbf{A})$  denote the maximum eigenvalue, the corresponding eigenvector of  $\mathbf{A}$ , and the matrix with columns being the eigenvectors corresponding to  $d$ -largest eigenvalues.  $\delta_{ij}$  is Kronecker delta, which takes value 1 when  $i = j$  and 0 otherwise.

## II. SYSTEM MODEL

Consider an IA-feasible MIMO interference channel [40]–[42] with  $K$  users as shown in Figure 1. Each user pair has  $M$  transmit antennas,  $N$  receive antennas and  $d$  independent data streams to be communicated. This system is represented by the notation  $(M \times N, d)^K$  [40]. Let  $\mathbf{x}_k$  of size  $d \times 1$  denote the transmit vector of the  $k^{\text{th}}$  user, distributed as  $\mathcal{CN}(\mathbf{0}, p_k \mathbf{I}_d)$  with power  $p_k = \frac{P_k}{d}$ , where  $P_k = \text{tr} \left( \mathbb{E} \left\{ \mathbf{x}_k \mathbf{x}_k^\dagger \right\} \right)$ ,  $\forall k$ . The MIMO channel matrix between the  $j^{\text{th}}$  transmitter and  $k^{\text{th}}$  receiver is denoted by  $\mathbf{H}_{kj} \in \mathbb{C}^{N \times M}$ . The received signal at the  $k^{\text{th}}$  user is given as

$$\mathbf{y}_k = \mathbf{H}_{kk} \mathbf{V}_k \mathbf{x}_k + \sum_{j \neq k} \mathbf{H}_{kj} \mathbf{V}_j \mathbf{x}_j + \mathbf{n}_k, \quad (1)$$

where the precoder  $\mathbf{V}_k = [\mathbf{v}_{k1}, \mathbf{v}_{k2}, \dots, \mathbf{v}_{kd}] \in \mathbb{C}^{M \times d}$  is an orthonormal matrix employed at the transmitter and satisfies the constraint  $\mathbf{v}_{ki}^\dagger \mathbf{v}_{kj} = \delta_{ij}$ ,  $\forall k, i, j$ . The quantity  $\mathbf{n}_k$  denotes zero mean additive white Gaussian noise (AWGN),

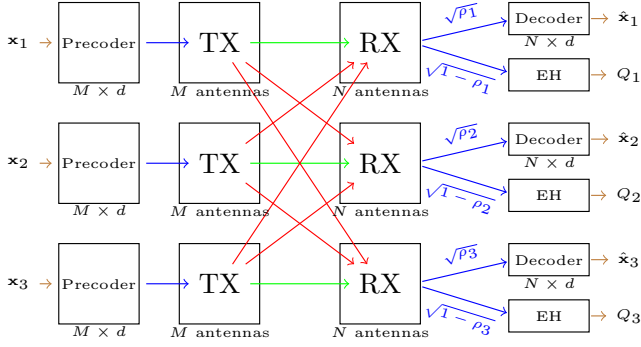


Figure 1.  $K = 3$  user interference channel  $(M \times N, d)^K$  with energy harvesters.

distributed as  $\mathcal{CN}(\mathbf{0}, \sigma^2 \mathbf{I}_N)$ . The first term in the above equation represents the desired signal component, while the second and third terms correspond to the interference and noise components respectively.

#### A. Information Decoding

Each receiver adaptively splits the received signal into two flows, i.e., one part goes to the RF-EH circuits for energy storage, while the other part is downconverted to for decoding the information. Let  $\rho_k \in [0, 1]$  be the power splitting ratio, which denotes the portion of the received signal power assigned for ID, and the remaining  $(1 - \rho_k)$  portion allocated for harvesting energy. Before ID, the split signal is further corrupted by additional circuit noise  $\mathbf{w}_k$ , due to the non-ideal splitters, non-ideal RF-to-baseband signal conversion, and thermal noise [11]. Therefore, after splitting, the signal for ID can be expressed as

$$\mathbf{y}_k^{ID} = \sqrt{\rho_k} \mathbf{y}_k + \mathbf{w}_k, \quad (2)$$

$$= \sqrt{\rho_k} \left( \mathbf{H}_{kk} \mathbf{V}_k \mathbf{x}_k + \sum_{j \neq k} \mathbf{H}_{kj} \mathbf{V}_j \mathbf{x}_j + \mathbf{n}_k \right) + \mathbf{w}_k, \quad (3)$$

where  $\mathbf{w}_k \sim \mathcal{CN}(\mathbf{0}, \delta^2 \mathbf{I}_N)$  represents the power splitting circuit noise vector at receiver  $k$ . The effective noise in the above equation can be written as  $\mathbf{n}_k + \frac{\mathbf{w}_k}{\sqrt{\rho_k}} \sim \mathcal{CN}(\mathbf{0}, \sigma_{ID}^2 \mathbf{I}_N)$ , where  $\sigma_{ID}^2 = \sigma^2 \left(1 + \frac{\delta^2}{\rho_k \sigma^2}\right)$ . Further, the signal is processed via a linear receiver  $\mathbf{U}_k$ , where  $\mathbf{U}_k = [\mathbf{u}_{k1}, \mathbf{u}_{k2}, \dots, \mathbf{u}_{kd}] \in \mathbb{C}^{N \times d}$  denotes an orthonormal decoding matrix, and can be obtained from minimizing MSE [21], [28].

*Remark:* For IA, it can be assumed that the CSI values  $(\mathbf{H}_{kj}, \forall j)$  are available at the  $k^{\text{th}}$  receiver. Receiver cooperation can be used to compute IA precoders and decoders, i.e., one node collects different CSIs, performs IA procedure, and then forwards the precoders/decoders to the respective nodes. This process is more energy efficient and requires a lower overhead [43].

1) *IA feasibility:* In the above equation, to cancel the interference component and preserve the desired signal, the

precoders  $\{\mathbf{V}_k, \forall k\}$  and the decoders  $\{\mathbf{U}_k, \forall k\}$  should be chosen to satisfy the following equations

$$\mathbf{U}_k^\dagger \mathbf{H}_{kj} \mathbf{V}_j = \mathbf{0}, \forall j \neq k \forall k, \quad (4)$$

$$\text{rank}(\mathbf{U}_k^\dagger \mathbf{H}_{kk} \mathbf{V}_k) = d, \forall k. \quad (5)$$

In order to find possible solutions for  $\{\mathbf{V}_k, \forall k\}$  and  $\{\mathbf{U}_k, \forall k\}$ , the system must be IA-feasible. Characterizations of IA-feasible systems are given in [40]–[42]. [40], and others [44]–[46] have demonstrated that feasible systems must necessarily be proper, which requires the number of equations in (4) to be lower than the number of variables, i.e.,  $M + N - (K + 1)d \geq 0$ . In addition to the proper condition, [41] has shown that feasibility can be verified by testing the surjectivity of the mapping proposed therein. More specifically, [42] and [44] have shown that a proper system is feasible when either  $M$  or  $N$  is divisible by  $d$ , or the system is symmetric, i.e.,  $M = N$ . Further, [47] presents a uniqueness condition and ensures the IA-feasibility and the global maximum sum rate (or minimum MSE). Thus, we utilize the condition

$$M + N - (K + 2)d \geq 0 \quad (6)$$

along with the IA algorithm from [47] to get the IA-solution.

2) *Sum rate:* The resulting sum rate at the  $k^{\text{th}}$  destination can be expressed as

$$R_k = \log_2 \left| \mathbf{I}_d + p_k \bar{\mathbf{H}}_{kk} \bar{\mathbf{H}}_{kk}^\dagger \left( \sigma_{ID}^2 \mathbf{I}_d + \sum_{\forall j \neq k} p_j \bar{\mathbf{H}}_{kj} \bar{\mathbf{H}}_{kj}^\dagger \right)^{-1} \right|, \quad (7)$$

where  $\bar{\mathbf{H}}_{kj} = \mathbf{U}_k^\dagger \mathbf{H}_{kj} \mathbf{V}_j$ . If the interference components are perfectly canceled i.e.  $\bar{\mathbf{H}}_{kj} = \mathbf{0}, \forall j \neq k$ , we have

$$R_{k,per} = \log_2 \left| \mathbf{I}_d + \frac{P_k}{d \sigma_{ID}^2} \bar{\mathbf{H}}_{kk} \bar{\mathbf{H}}_{kk}^\dagger \right| \quad (8)$$

$$= \sum_{i=1}^d \log_2 \left( 1 + \frac{P_k}{d \sigma_{ID}^2} |\sigma_{kki}|^2 \right), \quad (9)$$

where  $\sigma_{kki} \forall i = 1, \dots, d$  are the singular values of  $\bar{\mathbf{H}}_{kk}$ .

#### B. Harvested Energy

The second part of the splitted received signal for energy storage at receiver  $k$  can be written as

$$\mathbf{y}_k^{EH} = \sqrt{\bar{\rho}_k} \mathbf{y}_k, \forall k, \quad (10)$$

with  $\bar{\rho}_k = 1 - \rho_k$ . The corresponding average harvested energy that can be stored at receiver  $k$  can be expressed as

$$Q_k = \zeta \mathbb{E} \{ \|\mathbf{y}_k^{EH}\|^2 \} \quad (11)$$

$$\approx \zeta \bar{\rho}_k \sum_{j=1}^K \frac{P_j}{d} \|\mathbf{H}_{kj} \mathbf{V}_j\|_F^2, \quad (12)$$

where  $0 < \zeta < 1$  represents the power conversion efficiency for EH, which is assumed to be equal for all receivers in the paper. Note that the noise power  $\zeta(1 - \rho_k)N\sigma^2$  is negligible and hence, is omitted in the above equation.

### III. ENERGY OPTIMIZED PRECODING METHOD

In this section, we first derive the precoders that achieve the maximum value of harvested energy, followed by the rate-loss analysis via chordal distance.

#### A. Precoding for the maximum EH

The maximization problem for the total harvested energy with respect to precoders, subject to orthogonality constraints on the precoders can be cast as

$$\{\mathbf{V}_j^{EH}, \forall j\} = \arg \max_{\mathbf{V}_j, \forall j} \zeta \sum_k \bar{\rho}_k \sum_j \frac{P_j}{d} \|\mathbf{H}_{kj} \mathbf{V}_j\|_F^2 \quad (13a)$$

$$\text{subject to } \|\mathbf{V}_j\|_F^2 \leq d, \forall j. \quad (13b)$$

For each precoder, one can decouple the above problem, and the solution for the  $j^{\text{th}}$  precoder  $\mathbf{V}_j$  can be given using the dominant eigenvectors corresponding to  $d$  maximum eigenvalues of the  $\sum_k \bar{\rho}_k \mathbf{H}_{kj}^\dagger \mathbf{H}_{kj}$ , i.e.,

$$\begin{aligned} \mathbf{V}_j^{EH} &= \arg \max_{\|\mathbf{V}_j\|_F^2 \leq d} \text{tr} \left( \mathbf{V}_j^\dagger \mathbf{H}_j^\dagger \mathbf{H}_j \mathbf{V}_j \right) \quad (14) \\ &= \nu_{1:d} \left[ \mathbf{H}_j^\dagger \mathbf{H}_j \right] = \mathbf{W}_j^{[1]}, \end{aligned}$$

where  $\mathbf{H}_j^T = [\bar{\rho}_1 \mathbf{H}_{1j}^T, \dots, \bar{\rho}_K \mathbf{H}_{Kj}^T]$  denotes a stack of the channel matrices, and  $\mathbf{W}_j^{[1]}$  is computed via the eigenvalue decomposition (EVD) i.e.,

$$\mathbf{H}_j^\dagger \mathbf{H}_j = \sum_k \bar{\rho}_k \mathbf{H}_{kj}^\dagger \mathbf{H}_{kj} = \mathbf{W}_j \mathbf{\Lambda}_j \mathbf{W}_j^\dagger, \quad (15)$$

with  $\mathbf{W}_j = [\mathbf{W}_j^{[1]}, \mathbf{W}_j^{[2]}]$  and  $\mathbf{\Lambda}_j = \mathcal{D}(\lambda_{ji}, i = 1 \dots, M)$  such that  $\lambda_{j1} \geq \dots \geq \lambda_{jM}$  being in the descending order. The matrices  $\mathbf{W}_j^{[1]}$  and  $\mathbf{W}_j^{[2]}$  are orthonormal matrices of size  $M \times d$  and  $M \times M - d$ , respectively. In the following, we define chordal distance in order to analyze the rate loss.

#### B. Chordal Distance

**Definition 1.** For two orthonormal matrices  $\mathbf{V}, \hat{\mathbf{V}} \in \mathbb{C}^{M \times d}$  such that  $\hat{\mathbf{V}}^\dagger \hat{\mathbf{V}} = \mathbf{V}^\dagger \mathbf{V} = \mathbf{I}_d$ , the chordal distance between these matrices can be defined as

$$d_c^2(\hat{\mathbf{V}}, \mathbf{V}) = \frac{1}{2} \|\mathbf{V} \mathbf{V}^\dagger - \hat{\mathbf{V}} \hat{\mathbf{V}}^\dagger\|_F^2 = d - \|\mathbf{V}^\dagger \hat{\mathbf{V}}\|_F^2. \quad (16)$$

Note that the orthonormal matrices  $\mathbf{V}$  and  $\hat{\mathbf{V}}$  represent  $d$  dimensional subspaces of  $M$  dimensional space, i.e.,  $\mathbf{V}$  and  $\hat{\mathbf{V}}$  lie on a Grassmannian manifold  $\mathcal{G}_{M,d}$ , which is a collection of all such  $d$  dimensional subspaces. The chordal distance represents the distance between the subspaces spanned by these matrices. Thus, two orthonormal matrices who represent the same column space, will have zero distance. The CD value between two unit-norm vectors (say  $\mathbf{v}_1, \mathbf{v}_2 \in \mathcal{G}_{M,1}$ ), is equivalent to computing the inner-product between them, i.e.  $1 - |\mathbf{v}_1^\dagger \mathbf{v}_2|^2$ .

Further, given two matrices in  $\mathcal{G}_{M,d}$ , one matrix can be expressed into the other one via the CD decomposition from [25, Lemma 1]. The following lemma states the modified CD decomposition, where the modification comes from splitting

the null space of dimension  $M - d$  into a product of two variables.

**Lemma 2.** The two matrices  $\hat{\mathbf{V}}$  and  $\mathbf{V}$  (such that  $\hat{\mathbf{V}}^\dagger \hat{\mathbf{V}} = \mathbf{V}^\dagger \mathbf{V} = \mathbf{I}_d$ ) admits the following decomposition [25], [48, Lemma 1]

$$\mathbf{V} = \hat{\mathbf{V}} \mathbf{X} \mathbf{Y} + \hat{\mathbf{V}}^{\text{null}} \mathbf{S} \mathbf{Z}, \quad (17)$$

where  $\mathbf{V}, \hat{\mathbf{V}} \in \mathbb{C}^{M \times d}$ ,  $\hat{\mathbf{V}}^{\text{null}} = \text{null}(\hat{\mathbf{V}}_j) \in \mathbb{C}^{M-d \times d}$ ,  $\mathbf{X} \in \mathbb{C}^{d \times d}$  and  $\mathbf{S} \in \mathbb{C}^{M-d \times d}$  are orthonormal matrices,  $\mathbf{Y}, \mathbf{Z} \in \mathbb{C}^{d \times d}$  are upper triangular matrices with positive diagonal elements satisfying

$$\text{tr}(\mathbf{Z}^\dagger \mathbf{Z}) = d_c^2(\mathbf{V}, \hat{\mathbf{V}}) \quad (18)$$

$$\mathbf{Y}^\dagger \mathbf{Y} = \mathbf{I}_d - \mathbf{Z}^\dagger \mathbf{Z}, \quad (19)$$

Moreover,  $\mathbf{X}$  and  $\mathbf{Y}$  are distributed independent of each other, as is the pair  $\mathbf{S}$  and  $\mathbf{Z}$ .

*Proof:* A short proof is included in Appendix-A [25]. ■

It can be noted that this decomposition requires  $M \geq 2d$ , which is the case in interference alignment, wherein at least  $2d$  dimensions are required i.e., at least  $d$  dimensions for the desired signal and the remaining for the interference.

**Corollary 3.** For IC, if two sets of precoders have zero chordal distances, then the resulting rate and the harvested energy are same.

*Proof:* For two precoders  $\mathbf{V}_j$  and  $\hat{\mathbf{V}}_j$  such that  $\mathbf{V}_j = \hat{\mathbf{V}}_j \mathbf{X}_j \mathbf{Y}_j$  with  $\mathbf{X}_j \mathbf{X}_j^\dagger = \mathbf{Y}_j \mathbf{Y}_j^\dagger = \mathbf{I}_d, \forall j$ , the product  $\mathbf{V}_j \mathbf{V}_j^\dagger = \hat{\mathbf{V}}_j \hat{\mathbf{V}}_j^\dagger, \forall j$  will be same, resulting in the same sum rate and the harvested energy. ■

In the above, it can be noted that two orthogonal matrices with zero CD value will be termed as *equivalent* matrices, rather than considering the same matrix.

**Corollary 4.** Given an orthogonal matrix  $\mathbf{V}$  and the chordal distance value  $z$ , the displacement precoder (with respect to  $\mathbf{V}$ ) via the CD decomposition, can be obtained by relaxing the matrices  $\mathbf{Y}$  and  $\mathbf{Z}$  diagonal matrices  $\Sigma_Y$  and  $\Sigma_Z$  such that  $\Sigma_Y^2 = \mathbf{I}_d - \Sigma_Z^2$ , that is,

$$\mathbf{V}_D = \mathbf{V} \mathbf{X} \Sigma_Y + \mathbf{V}^{\text{null}} \mathbf{S} \Sigma_Z. \quad (20)$$

*Proof:* From Lemma 2, given the CD value  $z$ , the desired displacement matrix with respect to  $\mathbf{V}$  can be written as  $\mathbf{V} \bar{\mathbf{X}} \mathbf{Y} + \mathbf{V}^{\text{null}} \bar{\mathbf{S}} \mathbf{Z}$ . The chordal distance can then be equated as

$$z = d_c^2(\mathbf{V} \bar{\mathbf{X}} \mathbf{Y} + \mathbf{V}^{\text{null}} \bar{\mathbf{S}} \mathbf{Z}, \mathbf{V}) \quad (21a)$$

$$\stackrel{(a)}{=} d_c^2(\mathbf{V} \bar{\mathbf{X}} \mathbf{U}_Y \Sigma_Y \mathbf{V}_Y^\dagger + \mathbf{V}^{\text{null}} \bar{\mathbf{S}} \mathbf{U}_Z \Sigma_Z \mathbf{V}_Z^\dagger, \mathbf{V}) \quad (21b)$$

$$\stackrel{(b)}{=} d_c^2(\mathbf{V} \mathbf{X} \Sigma_Y + \mathbf{V}^{\text{null}} \mathbf{S} \Sigma_Z, \mathbf{V} \mathbf{V}_Y) \quad (21c)$$

$$\stackrel{(c)}{=} d_c^2(\mathbf{V} \mathbf{X} \Sigma_Y + \mathbf{V}^{\text{null}} \mathbf{S} \Sigma_Z, \mathbf{V}) \quad (21d)$$

$$= d_c^2(\mathbf{V}_D, \mathbf{V}), \quad (21e)$$

where in (a), the SVD is used for  $\mathbf{Z} = \mathbf{U}_Z \Sigma_Z \mathbf{V}_Z^\dagger$  and  $\mathbf{Y} = \mathbf{U}_Y \Sigma_Y \mathbf{V}_Y^\dagger$  with the same right singular vectors owing to the constraint  $\mathbf{Y}^\dagger \mathbf{Y} = \mathbf{I}_d - \mathbf{Z}^\dagger \mathbf{Z}$ ; in (b),  $\mathbf{S} = \bar{\mathbf{S}} \mathbf{U}_Z$ ,  $\mathbf{X} = \bar{\mathbf{X}} \mathbf{U}_Y$  are substituted; in (c), the fact that the chordal distance is unchanged for unitary multiplication  $\mathbf{V}_Y$ , is used, yielding that the matrices  $\mathbf{Z}$  and  $\mathbf{Y}$  can be relaxed to diagonal ones. ■

### C. Rate loss upper bound for EH based precoding

For the precoding in (14), the resultant maximum harvested energy can be given as the sum of the  $d$  dominant eigenvalues of  $\sum_k \bar{\rho}_k \mathbf{H}_{kj}^\dagger \mathbf{H}_{kj}$ . Note that the precoding in (14) does not consider the effect of interference on information decoding. However, the resulting precoders may partially align the interference. This partial interference alignment can be measured using the chordal distance value between EH precoders and the ideal IA precoders as

$$z_j^{EH} = d_c^2(\mathbf{V}_j, \mathbf{V}_j^{EH}), \forall j, \quad (22)$$

where  $\mathbf{V}_k, \forall k$  denote IA-precoders. The above chordal distance represents the displacement of  $\mathbf{V}_j^{EH}$  with respect to  $\mathbf{V}_j$ , and is independent of SNR values. The more the distance, the more will be interference, and the less will be the sum rates. Therefore, in the rate-energy trade-off, it is essential to specify the allowable sum rate losses in the system, which is characterized in the following result [28].

**Lemma 5. (Rate Loss Upper Bound (RLUB))** For an IC  $(M \times N, d)^K$ , employing an imperfect precoder at the source instead of IA precoder results in the rate loss  $\Delta R_k$ , the expected value of which can be bounded at the  $k^{th}$  receiver as

$$\mathbb{E}\{\Delta R_k\} < d \log_2 \left( 1 + \frac{P}{\sigma_{ID}^2} M_d \sum_{j \neq k} z_j \right), \quad (23)$$

with  $M_d = \frac{M}{d(M-d)}$ , and  $z_k = \mathbb{E}d_c^2(\mathbf{V}_k, \hat{\mathbf{V}}_k)$  being the average chordal distance between the imperfect precoder and the IA precoder.

*Proof:* Proof is given in Appendix-B [28, Lemma 4]. ■

### D. Problem Formulation

In literature for the SWIPT precoding [6], [49], an optimization problem is formulated, where a linear sum of the sum rate and sum harvested energy is maximized subjected to precoder constraints and quality-of-service constraints as

$$\max_{\mathbf{V}_j, \forall j} \sum_k R_k(\mathbf{V}_j, \forall j | \mathbf{H}_j) + \nu Q_k(\mathbf{V}_j, \forall j | \mathbf{H}_j) \quad (24a)$$

$$\text{subject to } \|\mathbf{V}_j\|_F^2 \leq d, \forall j, \quad (24b)$$

$$|R_j - \bar{R}_j| \leq d \log_2 c, \forall j, \quad (24c)$$

where  $\nu$  is the weight controlling the preferred objective; and  $\bar{R}_j$  and  $d \log_2 c$  are the rate and the rate-loss constraint.

Two objectives in the above are opposite in nature, i.e. sum rate maximization leads to reduced harvested energy, and the maximization of harvested energy degrades the sum rates. For the balanced precoding, we prioritize the sum rate maximized precoder i.e. IA precoder  $\mathbf{V}_j$ , and distort this precoder in such that the modified balanced precoder satisfies the required constraints. In general, if the IA precoder is degraded, it can result in severe rate losses, causing DoF loss. Thus, to displace the IA precoder in a systematic way, we utilize the chordal distance decomposition, in which the value of chordal distance decides the degradation of precoders, that is, DoF losses. From Lemma 5, it can be seen that if the distance is

chosen proportional to the inverse of SNR, only a constant rate loss is present, that is, there is no-loss of DoFs. This value of constant loss can be varied using the splitting ratio.

For example, to keep the RLUB a constant (say  $d \log_2 c$ ), the required CD value can be given as

$$z_k \leq \bar{z}(P) = \frac{c-1}{M_d(K-1)} \left( \frac{P}{\sigma_{ID}^2} \right)^{-1}, \quad (25)$$

which along with EH constraint can be written as

$$z_k \leq \min(\bar{z}(P), z_k^{EH}). \quad (26)$$

In the above, one should have  $\bar{z}(P) \leq z_k^{EH}$ ; otherwise, the sum rates would be worse due to the absence of IA, and in that case, the EH-maximizing precoder will be the better choice. In high SNR regime with analog feedback, these conditions can met easily, since the CD value is inversely proportional to SNR. In low and mid-SNR range, the value of splitting ratio  $\rho$  can be finely tuned to get the CD value  $z_k$  within the limit. Thus, given IA precoders and CD values with a specified constant RLUB, the balanced precoders are computed and analyzed in the following sections.

## IV. PROPOSED BALANCED PRECODING METHOD

Given the CD value  $\{z_j, \forall j\}$  and the IA precoders  $\{\mathbf{V}_j, \forall j\}$ , the objective of precoder optimization reduces to the maximization of the harvested energy, since the resulting sum rate with a given CD value provides fixed rate loss. Then using Corollary 4, the  $j^{th}$  balanced precoder can be given as

$$\mathbf{V}_j^{BAL} = \mathbf{V}_j \mathbf{X}_j \mathbf{Y}_j + \mathbf{V}_j^{\text{null}} \mathbf{S}_j \mathbf{Z}_j, \quad (27)$$

where the matrices  $\mathbf{Y}_j$  and  $\mathbf{Z}_j$  are diagonal;  $\mathbf{V}_j^{\text{null}}$  represents the left null space of  $\mathbf{V}_j$ , i.e.,  $\mathbf{V}_j^{\text{null}} = \text{null}(\mathbf{V}_j) \in \mathcal{G}_{M, M-d}$  and  $\mathbf{V}_j^{\text{null}\dagger} \mathbf{V}_j = \mathbf{0}$ .

The maximization problem for the total harvested energy with respect to finding the balanced precoding can be cast as

$$\max_{\mathbf{S}_j, \mathbf{Z}_j, \mathbf{X}_j, \mathbf{Y}_j, \forall j} \sum_k \zeta \bar{\rho}_k \sum_j \frac{P_j}{d} \|\mathbf{H}_{kj} \mathbf{V}_j^{BAL}\|_F^2 \quad (28a)$$

$$\text{subject to } \mathbf{V}_j^{BAL} = \mathbf{V}_j \mathbf{X}_j \mathbf{Y}_j + \mathbf{V}_j^{\text{null}} \mathbf{S}_j \mathbf{Z}_j, \forall j, \quad (28b)$$

$$\text{tr}(\mathbf{Z}_j \mathbf{Z}_j^\dagger) = \text{tr}(\mathbf{I} - \mathbf{Y}_j \mathbf{Y}_j^\dagger) \leq z_j, \forall j, \quad (28c)$$

$$\mathbf{Z}_j, \mathbf{Y}_j \text{ are diagonal matrices, } \forall j, \quad (28d)$$

$$\mathbf{X}_j^\dagger \mathbf{X}_j = \mathbf{X}_j \mathbf{X}_j^\dagger = \mathbf{I}, \forall j, \quad (28e)$$

$$\mathbf{S}_j^\dagger \mathbf{S}_j = \mathbf{I}, \forall j. \quad (28f)$$

It can be observed that one can decouple the above problem for each  $j^{th}$  precoder as

$$\max_{\mathbf{S}_j, \mathbf{Z}_j, \mathbf{X}_j, \mathbf{Y}_j} \|\mathbf{H}_j \mathbf{V}_j^{BAL}\|_F^2 \quad (29a)$$

$$\text{subject to } \mathbf{V}_j^{BAL} = \mathbf{V}_j \mathbf{X}_j \mathbf{Y}_j + \mathbf{V}_j^{\text{null}} \mathbf{S}_j \mathbf{Z}_j, \quad (29b)$$

$$\text{tr}(\mathbf{Z}_j \mathbf{Z}_j^\dagger) = \text{tr}(\mathbf{I} - \mathbf{Y}_j \mathbf{Y}_j^\dagger) \leq z_j, \quad (29c)$$

$$\mathbf{Z}_j, \mathbf{Y}_j \text{ are diagonal matrices,} \quad (29d)$$

$$\mathbf{X}_j^\dagger \mathbf{X}_j = \mathbf{X}_j \mathbf{X}_j^\dagger = \mathbf{I}, \quad (29e)$$

$$\mathbf{S}_j^\dagger \mathbf{S}_j = \mathbf{I}, \quad (29f)$$

, whose solution is computed as follows. We first obtain  $\mathbf{S}_j$ , followed by the computation of  $\mathbf{Z}_j$  and  $\mathbf{X}_j$ , which can be derived using either iterative or non-iterative method given below.

#### A. Getting $\mathbf{S}_j$

The objective function using the triangle inequality in (29a) can be bounded as

$$\begin{aligned} & \|\mathbf{H}_j (\mathbf{V}_j \mathbf{X}_j \mathbf{Y}_j + \mathbf{V}_j^{\text{null}} \mathbf{S}_j \mathbf{Z}_j)\|_F \\ & \leq \|\mathbf{H}_j \mathbf{V}_j \mathbf{X}_j \mathbf{Y}_j\|_F + \|\mathbf{H}_j \mathbf{V}_j^{\text{null}} \mathbf{S}_j \mathbf{Z}_j\|_F, \end{aligned} \quad (30)$$

where the equality occurs when both  $\mathbf{H}_j \mathbf{V}_j \mathbf{X}_j \mathbf{Y}_j$  and  $\mathbf{H}_j \mathbf{V}_j^{\text{null}} \mathbf{S}_j \mathbf{Z}_j$  have same directions or are proportional to each other. It can be noted that since both the matrix  $\mathbf{V}_j$  and its null space  $\mathbf{V}_j^{\text{null}}$  are present in the above expression, the equality cannot be achieved when  $z_j > 0$  or  $\mathbf{Z}_j \neq \mathbf{0}$ . Best efforts can be performed in order to align these two matrices via the following CD minimization problem as

$$\min_{\mathbf{S}_j, \mathbf{Z}_j, \mathbf{X}_j, \mathbf{Y}_j} d_c^2 (\mathbb{O}(\mathbf{H}_j \mathbf{V}_j \mathbf{X}_j \mathbf{Y}_j), \mathbb{O}(\mathbf{H}_j \mathbf{V}_j^{\text{null}} \mathbf{S}_j \mathbf{Z}_j)), \quad (31a)$$

$$\stackrel{(a)}{=} \min_{\mathbf{S}_j} d_c^2 (\mathbb{O}(\mathbf{H}_j \mathbf{V}_j), \mathbb{O}(\mathbf{H}_j \mathbf{V}_j^{\text{null}} \mathbf{S}_j)), \quad (31b)$$

$$\stackrel{(b)}{=} \max_{\mathbf{S}_j^{\dagger} \mathbf{S}_j = \mathbf{I}} \text{tr} \left[ \mathbf{D}_{V_j} \mathbf{V}_j^{\dagger} \mathbf{H}_j^{\dagger} \mathbf{H}_j \mathbf{V}_j^{\text{null}} \mathbf{S}_j \mathbf{D}_{V_{nj}} \right], \quad (31c)$$

where in (a), a property of orthogonalization is utilized; in (b), the definition of CD,  $\mathbb{O}(\mathbf{A}) = \mathbf{A} (\mathbf{A}^{\dagger} \mathbf{A})^{-1/2}$ ,  $\mathbf{D}_{V_j} = (\mathbf{V}_j^{\dagger} \mathbf{H}_j^{\dagger} \mathbf{H}_j \mathbf{V}_j)^{-1/2}$ , and  $\mathbf{D}_{V_{nj}} = (\mathbf{S}_j^{\dagger} \mathbf{V}_j^{\text{null}\dagger} \mathbf{H}_j^{\dagger} \mathbf{H}_j \mathbf{V}_j^{\text{null}} \mathbf{S}_j)^{-1/2}$  are substituted. From (b), the solution can be computed by selecting the columns in the same directions as  $\mathbf{V}_j^{\text{null}\dagger} \mathbf{H}_j^{\dagger} \mathbf{H}_j \mathbf{V}_j$  as

$$\mathbf{S}_j = \mathbb{O} \left( \mathbf{V}_j^{\text{null}\dagger} \mathbf{H}_j^{\dagger} \mathbf{H}_j \mathbf{V}_j \mathbf{D}_{V_j} \mathbf{D}_{V_{nj}} \right) \quad (32)$$

$$\equiv \mathbb{O} \left( \mathbf{V}_j^{\text{null}\dagger} \mathbf{H}_j^{\dagger} \mathbf{H}_j \mathbf{V}_j \right), \quad (33)$$

where the equivalence can be considered due to the fact that  $\mathbf{X}_j$ ,  $\mathbf{Y}_j$  and  $\mathbf{Z}_j$  are unknown (or yet to be designed based on  $\mathbf{S}_j$ ), and thus,  $\mathbf{S}_j$  can be independently computed first. Letting  $\mathbf{A}_j = \mathbf{V}_j^{\text{null}\dagger} \mathbf{H}_j^{\dagger} \mathbf{H}_j \mathbf{V}_j$ , the cross-term of two matrices reduces to

$$\text{tr} \left( \mathbf{Y}_j^{\dagger} \mathbf{X}_j^{\dagger} \mathbf{V}_j^{\dagger} \mathbf{H}_j^{\dagger} \mathbf{H}_j \mathbf{V}_j^{\text{null}} \mathbf{S}_j \mathbf{Z}_j \right) = \text{tr} \left( \mathbf{Z}_j \mathbf{Y}_j^{\dagger} \mathbf{X}_j^{\dagger} \left( \mathbf{A}_j^{\dagger} \mathbf{A}_j \right)^{1/2} \right).$$

#### B. Getting $\mathbf{Z}_j$ and $\mathbf{X}_j$ : an iterative approach

From (30), squaring the terms on both sides yields the Cauchy Schwarz's inequality

$$\Re \text{tr} \left( \mathbf{Y}_j^{\dagger} \mathbf{X}_j^{\dagger} \mathbf{V}_j^{\dagger} \mathbf{H}_j^{\dagger} \mathbf{H}_j \mathbf{V}_j^{\text{null}} \mathbf{S}_j \mathbf{Z}_j \right) \quad (34a)$$

$$\leq \|\mathbf{H}_j \mathbf{V}_j \mathbf{X}_j \mathbf{Y}_j\|_F \|\mathbf{H}_j \mathbf{V}_j^{\text{null}} \mathbf{S}_j \mathbf{Z}_j\|_F, \quad (34b)$$

which suggests that equivalently, the above cross-term can be maximized to get the maximum harvested energy.

Since the matrices  $\mathbf{Y}_j$  and  $\mathbf{Z}_j$  are relaxed to be diagonal, the matrix  $\mathbf{Y}_j = \mathcal{D}(y_{j1}, \dots, y_{jd})$  can be obtained from  $\mathbf{Z}_j = \mathcal{D}(z_{j1}, \dots, z_{jd})$  using the constraint in (28c) and (19) as

$$y_{ji} = +\sqrt{1 - z_{ji}^2}, \forall i = 1, \dots, d, \quad (35)$$

satisfying the constraint in (28c). The remaining components of the CD decomposition can be computed as the solution of the following optimization problem as

$$\max_{\mathbf{Z}_j, \mathbf{X}_j} \Re \text{tr} \left( \mathbf{Y}_j^{\dagger} \mathbf{X}_j^{\dagger} \mathbf{V}_j^{\dagger} \mathbf{H}_j^{\dagger} \mathbf{H}_j \mathbf{V}_j^{\text{null}} \mathbf{S}_j \mathbf{Z}_j \right),$$

which is a non-convex problem due to the product of  $\mathbf{Z}_j$  and  $\mathbf{X}_j$ . The efficient way to solve the problem is via an iterative method, where  $\mathbf{X}_j$  and  $\mathbf{Z}_j$  are solved alternately.

Given  $\mathbf{Z}_j$  and  $\mathbf{Y}_j$ , the optimization problem above can be reduced to a convex problem as

$$\max_{\mathbf{X}_j} \Re \text{tr} \left( \mathbf{Y}_j^{\dagger} \mathbf{X}_j^{\dagger} \mathbf{V}_j^{\dagger} \mathbf{H}_j^{\dagger} \mathbf{H}_j \mathbf{V}_j^{\text{null}} \mathbf{S}_j \mathbf{Z}_j \right) \quad (36a)$$

$$\text{subject to } \|\mathbf{X}_j\| \leq 1, \quad (36b)$$

where the spectral norm constraint above leads to the same constraint in (29e). The solution for  $\mathbf{X}_j$  can be obtained by choosing the same column directions as of  $\mathbf{V}_j^{\dagger} \mathbf{H}_j^{\dagger} \mathbf{H}_j \mathbf{V}_j^{\text{null}} \mathbf{S}_j \mathbf{Z}_j \mathbf{Y}_j^{\dagger}$ , i.e.,

$$\mathbf{X}_j = \left[ \frac{\mathbf{b}_1}{\|\mathbf{b}_1\|_2}, \dots, \frac{\mathbf{b}_d}{\|\mathbf{b}_d\|_2} \right] = \mathbf{B}_j \mathbf{D}_{B_j}^{-1}, \quad (37)$$

where  $\mathbf{B}_j = \mathbf{V}_j^{\dagger} \mathbf{H}_j^{\dagger} \mathbf{H}_j \mathbf{V}_j^{\text{null}} \mathbf{S}_j \mathbf{Z}_j \mathbf{Y}_j^{\dagger} = [\mathbf{b}_1, \dots, \mathbf{b}_d]$  and  $\mathbf{D}_{B_j} = \mathcal{D}(\|\mathbf{b}_1\|_2, \dots, \|\mathbf{b}_d\|_2) \succeq \mathbf{0}$ . Note that the above  $\mathbf{X}_j$  cannot be equivalently set to  $\mathbb{O} \left( \mathbf{V}_j^{\dagger} \mathbf{H}_j^{\dagger} \mathbf{H}_j \mathbf{V}_j^{\text{null}} \mathbf{S}_j \right)$ , since the above particular directions are important. Further, substituting  $\mathbf{X}_j$  in the trace yields the following result.

**Proposition 6.** *With the above selection of  $\mathbf{X}_j$ , the trace-value is non-negative*

$$\text{tr} \left( \mathbf{Y}_j^{\dagger} \mathbf{X}_j^{\dagger} \mathbf{V}_j^{\dagger} \mathbf{H}_j^{\dagger} \mathbf{H}_j \mathbf{V}_j^{\text{null}} \mathbf{S}_j \mathbf{Z}_j \right) = \text{tr} \left( \mathbf{B}_j^{\dagger} \mathbf{D}_{B_j}^{-1} \mathbf{B}_j \right) \geq 0,$$

where the equality occurs when  $z_j = 0$ .

Next, given  $\mathbf{Y}_j$ ,  $\mathbf{X}_j$  and  $z_j < z_j^{EH}$ , the diagonal matrix  $\mathbf{Z}_j$  can be updated as

$$\max_{\mathbf{Z}_j} \Re \text{tr} \left( \mathbf{Y}_j^{\dagger} \mathbf{X}_j^{\dagger} \mathbf{V}_j^{\dagger} \mathbf{H}_j^{\dagger} \mathbf{H}_j \mathbf{V}_j^{\text{null}} \mathbf{S}_j \mathbf{Z}_j \right) \quad (38a)$$

$$\text{subject to } \|\mathbf{Z}_j\|_F \leq \sqrt{z_j}, \quad (38b)$$

$$\mathbf{Z}_j \text{ is a diagonal matrix,} \quad (38c)$$

$$\mathbf{0} \preceq \mathbf{Z}_j \preceq \mathbf{I}, \quad (38d)$$

which is also a convex problem. We can equivalently recast the problem for  $\mathbf{z}_j^T = [z_{j1}, \dots, z_{jd}]$  as

$$\max_{\mathbf{z}_j} \mathbf{c}_j^T \mathbf{z}_j \quad (39a)$$

$$\text{subject to } \|\mathbf{z}_j\|_2 \leq \sqrt{z_j}, \quad (39b)$$

$$0 \leq z_{j,i} \leq 1, \forall i = 1, \dots, d, \quad (39c)$$

where the vector  $\mathbf{c}_j = [c_{j1}, \dots, c_{jd}]$  and  $c_{ji} = \left[ \mathbf{Y}_j^{\dagger} \mathbf{X}_j^{\dagger} \mathbf{V}_j^{\dagger} \mathbf{H}_j^{\dagger} \mathbf{H}_j \mathbf{V}_j^{\text{null}} \mathbf{S}_j \right]_{i,i}$ ,  $\forall i = 1, \dots, d$ . The values  $c_{ji}, \forall i$  are real and non-negative from the proposition 6. The solution



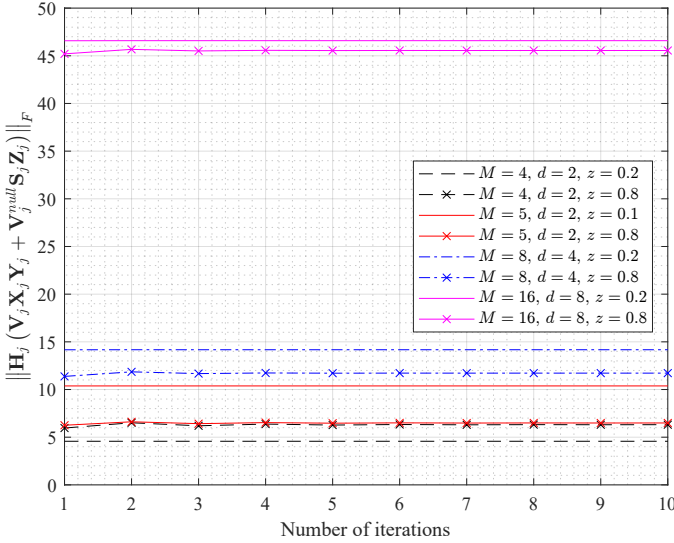


Figure 2. Norm value versus the number of iterations for different interference channels and different values of chordal distance.

of the above problem is given by choosing  $\mathbf{z}_j$  equal to  $\mathbf{c}_j$  and scaling it to satisfy the norm constraint. Thus, we write  $z_{ji} = \min\left(\sqrt{z_j} \frac{c_{ji}}{\|\mathbf{c}_j\|}, 1\right)$ , and normalize the resulting entries to satisfy  $\sum_{i \in \mathcal{I}} z_{ji}^2 = z_j - (d - |\mathcal{I}|)$ , where  $\mathcal{I} = \{i : z_{ji} < 1\}$ , i.e.,  $z_{ji} \leftarrow \frac{z_{ji}}{\sum_{i \in \mathcal{I}} z_{ji}^2} \sqrt{z_j - (d - |\mathcal{I}|)}, \forall i \in \mathcal{I}$ .

### C. Algorithm

---

#### Algorithm 1 Iterative CD decomposition procedure.

---

**Input:**  $\mathbf{H}_j$ ,  $\mathbf{V}_j$  and  $z_j$ .

**Output:**  $\mathbf{V}_j^{BAL}$ .

- 1: **if**  $z_j > z_j^{EH}$  **then**
  - 2:     Return  $\mathbf{V}_j^{BAL} = \mathbf{V}_j^{EH}$ .
  - 3: **else**
  - 4:     Compute  $\mathbf{S}_j = \mathbb{O}\left(\mathbf{V}_j^{\text{null}\dagger} \mathbf{H}_j^\dagger \mathbf{H}_j \mathbf{V}_j\right)$ .
  - 5:     Initialize  $\mathbf{Z}_j = \sqrt{\frac{z_j}{d}} \mathbf{I}$  and  $\mathbf{Y}_j$  by (35).
  - 6:     Solve (36a) to get  $\mathbf{X}_j$ .
  - 7:     Solve (38a) to get  $\mathbf{Z}_j$ .
  - 8:     Get  $\mathbf{Y}_j$  by (35).
  - 9:     Go to step 6 until convergence.
  - 10:    Return  $\mathbf{V}_j^{BAL}$  via (29b).
  - 11: **end if**
- 

Now, with all components obtained, the resulting balanced precoder can be computed via (29b). The summary of this procedure is given in Algorithm 1. If  $z_j > z_j^{EH}$ , we choose energy optimized precoder as the balanced precoder  $\mathbf{V}_j^{BAL} = \mathbf{V}_j^{EH}$ . Regarding the convergence, it can be seen that since both  $\mathbf{Z}_j$  and  $\mathbf{X}_j$  maximize the same linear objective, thus convergence is guaranteed with a global optimum value, as plotted in Figure 2. Regarding the number of iterations, we observe via simulations that it takes only a few (4 to 8) iterations to converge.

### D. Getting $\mathbf{Z}_j$ and $\mathbf{X}_j$ : a non-iterative approach

Here, we present a suboptimal non-iterative method to compute  $\mathbf{X}_j$  and  $\mathbf{Z}_j$ . This method is based on upper bound in the equation (30). In (30), applying the max-operator on both sides yields

$$\begin{aligned} & \max_{\mathbf{S}_j, \mathbf{Z}_j, \mathbf{X}_j, \mathbf{Y}_j} \left\| \mathbf{H}_j (\mathbf{V}_j \mathbf{X}_j \mathbf{Y}_j + \mathbf{V}_j^{\text{null}} \mathbf{S}_j \mathbf{Z}_j) \right\|_F \\ & \leq \max_{\mathbf{X}_j, \mathbf{Y}_j} \left\| \mathbf{H}_j \mathbf{V}_j \mathbf{X}_j \mathbf{Y}_j \right\|_F + \max_{\mathbf{S}_j, \mathbf{Z}_j} \left\| \mathbf{H}_j \mathbf{V}_j^{\text{null}} \mathbf{S}_j \mathbf{Z}_j \right\|_F, \end{aligned} \quad (40)$$

Thus, for a lower complexity solution, we solve the right hand side get the components for the balanced precoding.

Given  $z_j < z_j^{EH}$ , the matrix  $\mathbf{Z}_j$  can be obtained to maximize the harvested power as

$$\mathbf{Z}_j = \arg \max_{\mathbf{Z}_j \succ \mathbf{0}} \left\| \mathbf{H}_j \mathbf{V}_j^{\text{null}} \mathbf{S}_j \mathbf{Z}_j \right\|_F^2 \quad (41)$$

subject to (38b), (38c), (38d).

The above problem can be simplified as

$$\max_{0 \leq z_{ji} \leq 1, \forall i} \sum_i z_{ji}^2 f_{ji} \quad (42a)$$

$$\text{subject to } \sum_i z_{ji}^2 \leq z_j, \quad (42b)$$

where the values  $f_{ji} = \left[ \mathbf{S}_j^\dagger \mathbf{V}_j^{\text{null}\dagger} \mathbf{H}_j^\dagger \mathbf{H}_j \mathbf{V}_j^{\text{null}} \mathbf{S}_j \right]_{i,i}, \forall i = 1, \dots, d$  are real and non-negative. For the solution of the above optimization, we write

$$z_{ji}^2 = \min \left( z_j \frac{f_{ji}}{\sum_i f_{ji}}, 1 \right), \forall i = 1, \dots, d, \quad (43)$$

and normalize the resulting entries ( $\mathcal{I} = \{i : z_{ji} < 1\}$ ) to satisfy  $\sum_{i \in \mathcal{I}} z_{ji}^2 = z_j - (d - |\mathcal{I}|)$ .

Next, the matrix  $\mathbf{Y}_j$  can be computed using (35). Further, the matrix  $\mathbf{X}_j$  can be chosen as

$$\mathbf{X}_j = \arg \max_{\|\mathbf{X}_j\| \leq 1} \left\| \mathbf{H}_j \mathbf{V}_j \mathbf{X}_j \mathbf{Y}_j \right\|_F^2 \quad (44)$$

$$= \bar{\mathbf{B}}_j \bar{\mathbf{D}}_{B_j}^{-1}, \quad (45)$$

where  $\bar{\mathbf{B}}_j = \mathbf{V}_j^\dagger \mathbf{H}_j^\dagger \mathbf{H}_j \mathbf{V}_j \mathbf{Y}_j^{-1} = [\bar{\mathbf{b}}_1, \dots, \bar{\mathbf{b}}_d]$  and  $\bar{\mathbf{D}}_{B_j} = \mathcal{D}(\|\bar{\mathbf{b}}_1\|_2, \dots, \|\bar{\mathbf{b}}_d\|_2)$ . The resulting  $j^{\text{th}}$  precoder  $\mathbf{V}_j^{BAL}$  can be given via (29b).

### E. Computational complexity

The product  $\mathbf{H}_j^\dagger \mathbf{H}_j$  need  $\mathcal{O}(M^2 NK)$  operations. For  $\mathbf{S}_j$ , the product and  $\mathbb{O}(\cdot)$  need  $\mathcal{O}(NK \cdot M(M-d) + NKd \cdot M + NK(M-d) \cdot M) = \mathcal{O}(NKM^2)$  and  $\mathcal{O}(d^2 \cdot (M-d) + d^3) = \mathcal{O}(Md^2)$ , respectively. The rest of operations are below  $\mathcal{O}(Md^3)$  or  $\mathcal{O}(M^3)$ . Thus, if  $M = N$ , Algorithm 1 has  $\mathcal{O}(M^3K + Md^2N_I) \approx \mathcal{O}(M^3K)$  computational complexity, where the number of iterations  $N_I$  for convergence are few (4-8), i.e.  $N_I \ll \frac{KM^2}{d^2}$ . Similarly, non-iterative process has the similar complexity. Therefore, the main computational intensive process is to compute the products of matrices, e.g.,  $\mathbf{H}_j^\dagger \mathbf{H}_j$  or  $\mathbf{V}_j^{\text{null}\dagger} \mathbf{H}_j^\dagger \mathbf{H}_j \mathbf{V}_j$ .

### F. Bounds on the harvesting Energy

It can be noted from the above analysis that not any trivial balanced precoding can provide the better harvested energy. For the proposed balanced precoding, the following bounds can be computed.

**Lemma 7.** *Given the balanced precoders  $\{\mathbf{V}_k^{BAL}, \forall k\}$  and IA precoders  $\{\mathbf{V}_k, \forall k\}$  for the channel  $\{\mathbf{H}_{kj}, \forall k, j\}$ , the total harvested energy can be bounded as*

$$\zeta \sum_{j=1}^K \frac{P_j}{d} \left[ \|\mathbf{H}_j \mathbf{V}_j\|_F^2 \left(1 - \frac{z_j}{d}\right) + \|\mathbf{H}_j \mathbf{V}_j^n\|_F^2 \left(\frac{z_j}{d}\right) \right] \quad (46a)$$

$$\leq \sum_{k=1}^K Q_k(\bar{\rho}_k, \mathbf{V}_k^{BAL}) \leq \zeta \sum_{j=1}^K P_j \lambda_{j1}, \quad (46b)$$

where the left and right equalities occur for  $z_j = 0$  and  $z_j = z_j^{EH}$  respectively.

*Proof:* Proof is given in Appendix-C. ■

The above result shows an improvement over (12) based on the value of  $z_j$ , i.e., the balanced precoding guarantees the better harvested energy than that achieved using just perfect IA precoders. With the balanced precoding, the resultant rate loss can be obtained from the upper bound in the Lemma 5.

With  $\bar{\rho}_k = \bar{\rho}, \forall k$  and with  $\mathcal{CN}(0, 1)$  entries in  $\mathbf{H}_{kj}$ , performing the expectation on both the sides in the above equation gives

$$\zeta \bar{\rho} K N \sum_j P_j \approx \sum_{k=1}^K \mathbb{E}\{Q_k(\bar{\rho})\} \quad (47a)$$

$$\leq \zeta \bar{\rho} K N d \left( \frac{KN + d}{KNd + 1} \right)^{2/3} \sum_{j=1}^K P_j, \quad (47b)$$

where the left approximation is obtained assuming  $\mathbb{E}\|\mathbf{H}_j \mathbf{V}_j^{BAL}\|_F^2 \approx \bar{\rho} K N d$ , and the right inequality is given by  $\mathbb{E}\{\lambda_{j1}\} = \bar{\rho} K N d \left( \frac{KN + d}{KNd + 1} \right)^{2/3}$  [50].

## V. ENERGY HARVESTING WITH FEEDBACK

In the above formulation for EH, perfect IA precoder has been employed, which is not the case in practice. In practice, to avail the precoder at the transmitter side, either CSI or precoder is fed back in quantized or analog form. In this section, considering precoder feedback, the sum rate and energy harvesting terms are analyzed. Recall that the trade off between these is characterized by the chordal distance. Therefore, in the following analog precoder feedback scheme is provided, followed by limited precoder feedback.

### A. Analog Feedback

In analog feedback, after the estimation of the reverse links, full  $(M \times d)$  precoder is sent back using analog transmission [28]. For orthogonal transmissions, destinations transmit simultaneously in  $Kd$  time slots respectively. After receiving the noisy precoder information at the sources, the orthogonalization of the MMSE estimate is performed to obtain the final precoder estimate.

From the results in [28], it can be observed that for lower feedback SNR, the average chordal distance between the estimate and IA precoder remains constant, which results in the sum rate loss increasing with SNR (see Lemma 5). On the other hand, for medium to high SNR case, the chordal distance decreases inversely proportional to SNR, which keeps the rate loss constant for this SNR range. In IA scenarios, the medium to high SNR regime is of more importance. In conjunction with energy harvesting, one can note that the chordal distance is automatically set according to the feedback SNR selected at the destinations. The conclusion of this result is that analog feedback also helps in increasing energy efficiency while maintaining linear sum rate scaling, that is, no-loss of DoFs. To get the desired energy in harvesting, only the splitting factor needs to be selected using the results in the previous section.

### B. Quantized Feedback

Let the vector  $\mathbf{b} = [b_1, b_2, \dots, b_K]^T$  denote the number of feedback bits allocated for each user. The corresponding precoder quantization codebook of size  $2^{b_k}$  is given as  $\mathcal{C}(b_k) = \{\mathbf{C}_1(b_k), \dots, \mathbf{C}_{2^{b_k}}(b_k)\}$  where each entry  $\mathbf{C}_i(b_k)$  is an  $M \times d$  orthogonal matrix such that  $\mathbf{C}_i(b_k)^\dagger \mathbf{C}_i(b_k) = \mathbf{I}_d$ . The codebook  $\mathcal{C}(b_k)$  is considered known to all the transmitters and receivers. The precoder matrix index (PMI) vector is denoted as  $\mathbf{q} = [q_1, \dots, q_K]^T$  with each  $q_k$  representing an index from the codebook  $\mathcal{C}(b_k)$ , i.e.  $1 \leq q_k \leq 2^{b_k}, \forall k$ .

In the conventional method, when the perfect IA precoders are available, each of the precoders is quantized using the chordal distance metric. Let  $\mathbf{q}_{CD}$  denote the PMI vector obtained using quantization based on chordal distance. The  $k^{th}$  index of  $\mathbf{q}_{CD}$  is obtained as

$$q_{CD,k} = \arg \min_{\mathbf{C}_i \in \mathcal{C}} d_c^2(\mathbf{V}_k, \mathbf{C}_i), \quad (48)$$

where  $q_{CD,k}$  is the index of the closest codebook entry. This technique incurs a low computational complexity. Improved precoder feedback schemes can be seen in [29], [30] which suggest that the sum rate can be improved for the same number of quantization bits. The main point is to observe that the limited feedback can increase the harvested energy since chordal distance is non-zero. Note that the resultant chordal distance of quantized precoders varies inversely proportional to the codebook size, i.e., as codebook size increases EH decreases and sum rate increases. Therefore, given the codebook  $\mathcal{C}(b_k)$ , the chordal distance can be fixed as

$$z = \mathbb{E} d_c^2(\mathbf{V}_k, \mathbf{C}_i) < 2^{-\frac{b_k}{d(M-d)}}, \quad (49)$$

and splitting ratio can be varied to get the desired harvested energy.

*Remark (SNR shift):* For  $z = 0$ , the splitting causes the noise variance to change from  $\sigma^2$  to  $\sigma_{ID}^2$ , which causes the  $\left(\frac{\sigma_{ID}^2}{\sigma^2}\right)_{dB} = \left(1 + \frac{\delta^2}{\rho_k \sigma^2}\right)_{dB}$  shift in SNR without losing linear sum rate scaling. It shows that the splitting factor can be obtained for a given SNR shift or a given constant rate loss. For example, to get only 3 dB loss in sum rates,  $1 + \frac{\delta^2}{\rho_k \sigma^2} = 2$  or  $\rho_k = 1 - \frac{\delta^2}{\sigma^2}$ .



## VI. SIMULATION RESULTS

### A. Simulation settings

The value of essential variables are given as follows:  $\rho_k = \zeta = 0.5, \forall k$ ,  $P_k = P$  and  $z_j = z$ . We consider two IA-feasible systems (a)  $(4 \times 4, 2)^3$  and (b)  $(5 \times 5, 2)^3$ . Each entry of  $\mathbf{H}_{k,j}$  is assumed to be distributed as  $\mathcal{CN}(0, 1)$ . For balanced precoding, the iterative process (ICD) is run for a maximum of 6 iterations. We assume for all  $j$ ,  $z_j = z < \min_j z_j^{EH}$ . In the following figures, we compare different precoding strategies given below.

- (RAND) Random full rank precoder with orthogonal columns;
- (MAX-EH) Harvested energy maximizing precoder;
- (SSIA) Balanced Precoders from subspace IA method with  $z = 0, 0.1, 0.8$ ;
- (MSEIA) Balanced precoder from MMSE based IA algorithm [47] with  $z = 0, 0.1, 0.8$ ;
- (PQFB) Precoder obtained from quantized feedback from a given codebook of size 8 bits [47];
- Precoder acquired via analog precoder feedback (PAFB) [28], and via analog CSI feedback (CSIAFB) [51] with similar feedback transmission power as the forward one,  $P_f = P$ .

### B. Rate-energy region plots

Given the precoders  $\{\mathbf{V}_k, \forall k\}$ , the rate-energy region can be written as [52], [53],  $\mathcal{C} =$

$$\bigcup_{\rho} \left\{ (R, Q) : R \leq \sum_{k=1}^K R_k(\rho_k, \mathbf{V}_k), Q \leq \sum_{k=1}^K Q_k(\rho_k, \mathbf{V}_k) \right\}, \quad (50)$$

where  $\rho = [\rho_1, \dots, \rho_K]$  is a vector of  $K$  splitting factors. For a splitting noise variance  $\delta^2 = 0.1$ , assuming  $\rho_k = \rho, \forall k$  varying  $\rho$  from 0 to 1, the parametric plots are drawn to illustrate rate-energy regions [52], [53].

Figure 3 shows the sum rate versus the total harvested energy plot for three types of precoders, viz., MSE-IA, MAX-EH, and MSE-IA with balanced precoding with different values of CD. It can be seen that MSE-IA region has higher sum rates and lower energies, while the region for MAX-EH precoders has less sum rates and higher energies. These plots represent two extreme ends of rate and energy achievability. Next, for the balanced precoding with iterative method, it can be observed that as  $z$  increases, the rate decreases and energy increases, when  $z < \min_j z_j^{EH}$ . When  $z > \min_j z_j^{EH}$ , both rate and energy achieved are lower. Therefore, for the case of  $z > \min_j z_j^{EH}$ , it is better to employ MAX-EH precoder than IA-precoder.

Figure 4 compares the same rate-energy region for different precoding schemes. The following points can be concluded from the figure.

- $\mathcal{C}_{\text{RAND}} \subset \mathcal{C}_{\text{MAX-EH}}$  and  $\mathcal{C}_{\text{RAND}} \subset \mathcal{C}_{\text{MSEIA-ICD}}$ : Random precoders have worst rates.
- $\mathcal{C}_{\text{SSIA}} \subset \mathcal{C}_{\text{MSEIA}}$ : Among IA-methods, MSE based methods are better suited for both rate and energy optimization.

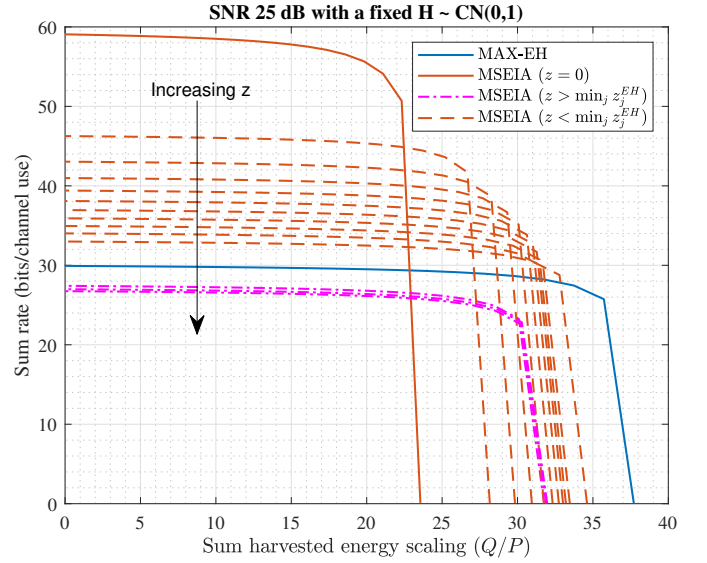


Figure 3. Rate-energy plot for  $(5 \times 5, 2)^3$  system for iterative CD based balanced precoding.

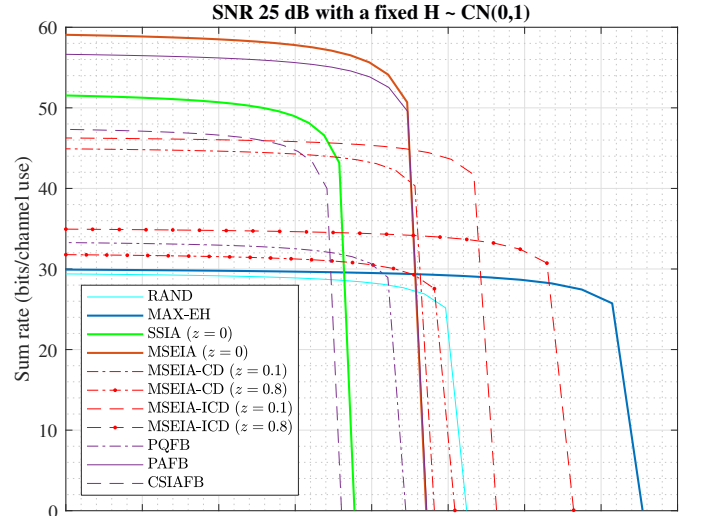


Figure 4. Rate-energy plot for  $(5 \times 5, 2)^3$  system for different precoding methods.

- $\mathcal{C}_{\text{CSIAFB}} \subset \mathcal{C}_{\text{PAFB}}$  and  $\mathcal{C}_{\text{PQFB}} \subset \mathcal{C}_{\text{PAFB}}$ : Analog precoder feedback is better than both analog CSI feedback and precoder quantized feedback.
- $\mathcal{C}_{\text{MSEIA-CD}} \subset \mathcal{C}_{\text{MSEIA-ICD}}$ : Iterative balanced precoding method provides better rate and energy than that via non-iterative one. Therefore, in the following, iterative method based precoding is considered for comparison.

### C. Sum Rate and harvested energy versus SNRs

Figure 5-6 illustrate the sum rates with respect to SNR for  $(4 \times 4, 2)^3$  and  $(5 \times 5, 2)^3$  systems, respectively. It can be observed that both SSIA and MSEIA ( $z = 0$ ) achieve linear sum rate scaling with SNR, while with  $z > 0$ , saturating sum rates are obtained at high SNR. As compared to  $(4 \times 4, 2)^3$  system, the saturation in sum rates starts at higher SNR for  $(5 \times 5, 2)^3$  system, since more spatial dimensions are

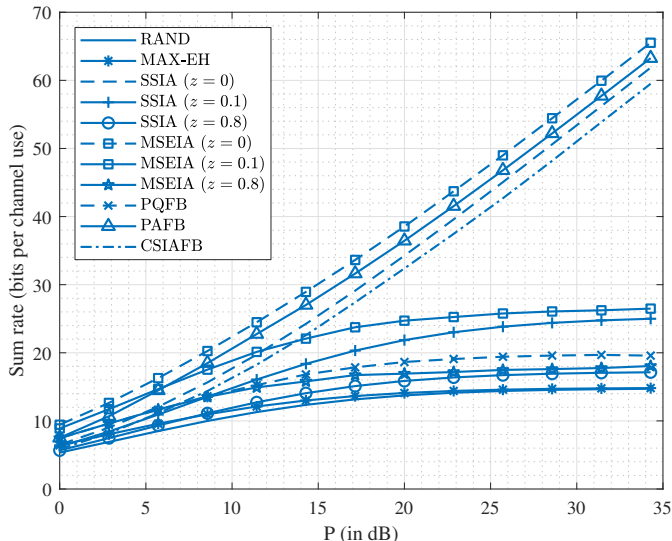


Figure 5. Sum rates versus SNR with  $(4 \times 4, 2)^3$  system.

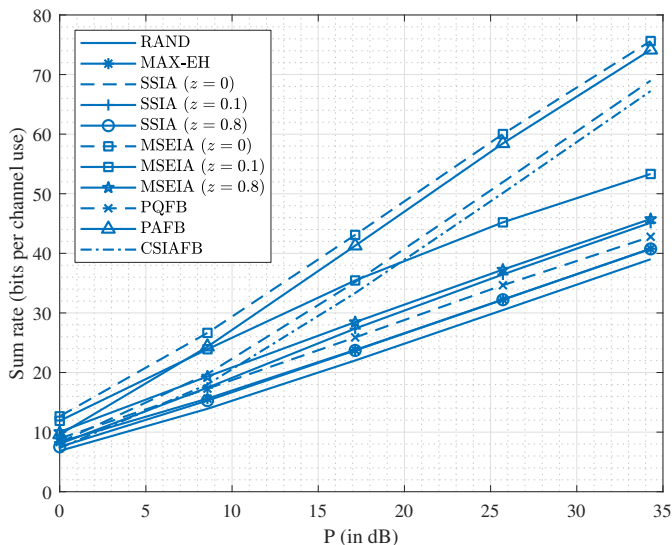


Figure 6. Sum rates versus SNR with  $(5 \times 5, 2)^3$  system.

available in  $(5 \times 5, 2)^3$  to grant diversity gains. For limited feedback with 8 quantization bits per precoder, similar rate losses can be seen due to saturation, because to keep the rate loss constant number of bits need to be scaled proportional to SNR [47]. For analog feedback (AFB) schemes (CSIAFB and PAFB), a constant rate loss can be observed at high SNR regime, yielding the better performance than quantization schemes. Figure 6 plots the similar trend for  $(5 \times 5, 2)^3$  system, except that higher sum rates are achieved due to more spatial dimensions. The decreasing/saturating behavior of sum rates Figure 5 can also be observed in Figure 6; however, it requires much higher SNR in the  $(5 \times 5, 2)^3$  system than the SNR in  $(4 \times 4, 2)^3$  system.

#### D. Rate-Energy performance versus chordal distance

Figure 7 plots the sum rate (left-axis) and the harvested energy (right-axis) versus the squared chordal distance  $z =$

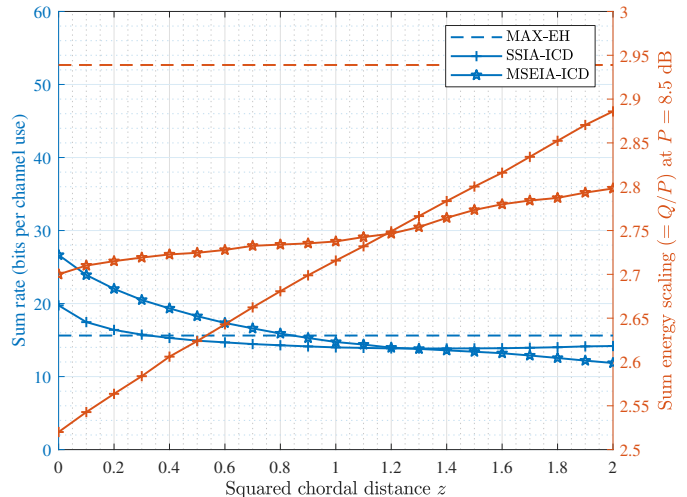


Figure 7. Figure illustrates both the sum rate and sum harvested power variations versus chordal distance for  $(5 \times 5, 2)^3$  at 25 dB SNR.

$d_c^2(\mathbf{V}_j, \mathbf{V}_j^{BAL}), \forall j$  required for the balanced precoding with MSE-IA and SS-IA. It can be seen that the sum rate decreases in a logarithmic manner as  $z$  increases. This behavior has been analyzed in the Equation (23) for rate-loss upper bound. On the other hand, harvested energy is increased, if  $z$  is increased. Upto a certain value of  $z$  (say  $z_{th}$ ), MSE-IA provides higher energies than that with SS-IA. When  $z > z_{th}$ , SS-IA yields better energy output. Regarding the sum rate intersection between MAX-EH and MSE-IA (or SS-IA), it is the point when  $z = \min_j z_j^{EH}$ . When  $z > \min_j z_j^{EH}$ , both rate and energy are lower than that of MAX-EH. Thus, it is better to consider MAX-EH precoder beyond this intersection. Note that the earlier intersection of SS-IA than MSE-IA is due to the fact that MSE-IA provides better sum rates than SS-IA in general.

#### E. Energy scaling with SNRs

The respective harvested energy scaling (with respect to transmit power ( $P$ )) is illustrated in Figure 8 for different precoding strategies. Max-EH precoding provides maximum scaling. MSE-IA methods provide better scaling than SS-IA based ones. Also, for rate-energy balanced precoding, increasing the chordal distance shows increase in scaling. This result is also depicted in Figure 7, which shows the sum rate and EH scaling variations with respect to chordal distance. It can be seen that the energy scales linearly with chordal distance. The most efficient method is PAFB, where the chordal distance is selected automatically inversely proportional to feedback SNR. It suggests to choose the chordal distance carefully based on SNR and the required harvested energy constraint.

#### F. SER plots

Figure 9 depicts the average SER plots with QPSK modulation for  $(5 \times 5, 2)^3$ . It can be seen that perfect IA precoders ( $z = 0$ ) achieve the minimum SER, while with  $z = 0.1, 0.8$ , the SER saturates. For quantization based methods, the SER can be seen to be higher. Among the feedback schemes,

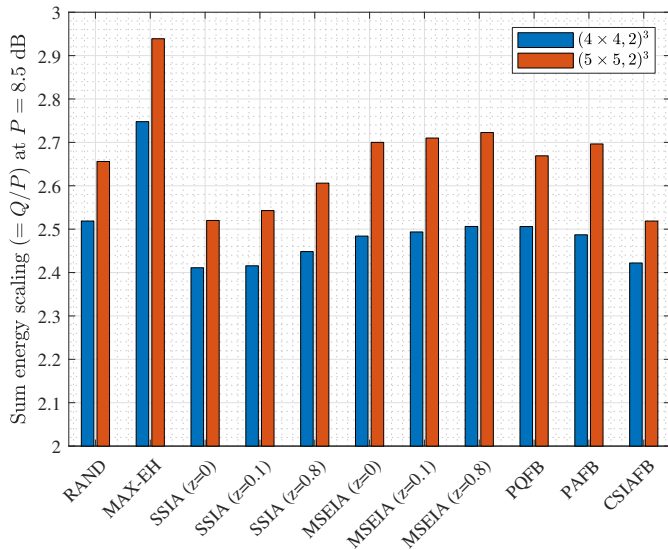


Figure 8. Figure showing the sum harvested power scaling for different precoding methods for  $(4 \times 4, 2)^3$  and  $(5 \times 5, 2)^3$  systems at 25 dB SNR.

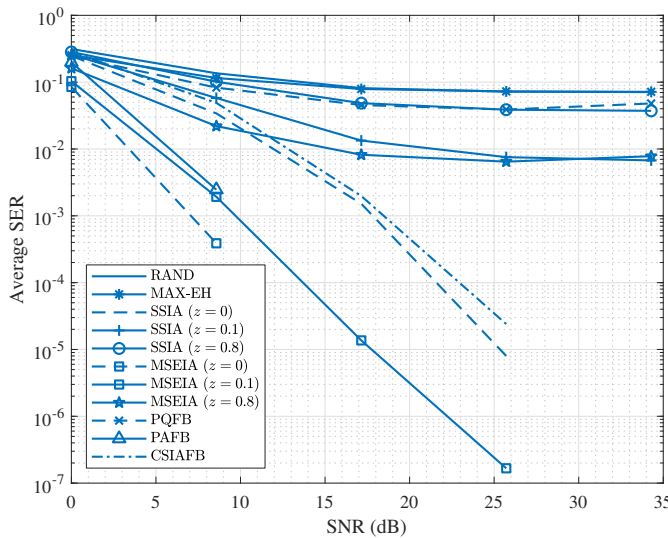


Figure 9. Figure depicts the average QPSK symbol error rate (SER) with respect to SNR for  $(5 \times 5, 2)^3$ .

PAFB methods can be seen to provide a significantly better SER, close to perfect MSE-IA scheme. More importantly, PAFB methods also yield linear sum rate scaling and EH scaling approximately to MSE-IA ( $z = 0.1$ ), which shows the effectiveness of PAFB schemes.

## VII. CONCLUSION

In this paper, we have provided a low-complexity systematic balanced precoding method towards getting the improved trade-off between sum rate and harvested energy. First, the precoder that achieves maximum harvested energy has been computed. Thereafter, utilizing the CD decomposition, we have systematically derived and analyzed the proposed precoder for SWIPT trade-off. The lower and upper bounds on harvested energy for this construction have been obtained. Due

to the dependence on CD, the relations to the analog and quantized feedback schemes have been discussed. Simulation results show that MSE based methods are better for SWIPT than subspace alignment method or leakage minimization algorithm. Among feedback schemes, PAFB has shown to improve sum rates without losing the linear scaling (with SNR) as well as improved harvested energy.

The future work is to investigate the proposed schemes in case of hybrid precoding with non-linear hardware impairments and constraints.

## APPENDICES

### A. Proof of CD decomposition

Consider two  $M \times d$  orthonormal matrices  $\mathbf{V}, \hat{\mathbf{V}}$  such that  $\mathbf{V}^\dagger \mathbf{V} = \hat{\mathbf{V}}^\dagger \hat{\mathbf{V}} = \mathbf{I}_d$ . Its left null space of size  $M \times M - d$  can be represented as  $\hat{\mathbf{V}}_j^{\text{null}} = \text{null}(\hat{\mathbf{V}}_j)$ . Then, we can write

$$\mathbf{V} = \hat{\mathbf{V}} \hat{\mathbf{V}}^\dagger \mathbf{V} + (\mathbf{I}_M - \hat{\mathbf{V}} \hat{\mathbf{V}}^\dagger) \mathbf{V} \quad (51)$$

$$= \underbrace{\hat{\mathbf{V}} \hat{\mathbf{V}}^\dagger \mathbf{V}}_{=\mathbf{X}\mathbf{Y}} + \underbrace{\hat{\mathbf{V}}^{\text{null}} \hat{\mathbf{V}}^{\text{null}\dagger} \mathbf{V}}_{=\mathbf{S}\mathbf{Z}} \quad (52)$$

where the last equation is obtained by the QR-decomposition such that  $\mathbf{X}$  and  $\mathbf{S}$  are  $d \times d$  and  $M - d \times d$  orthonormal matrices respectively. It verifies  $d_c^2(\mathbf{V}, \hat{\mathbf{V}}) = d - \|\hat{\mathbf{V}}^\dagger \mathbf{V}\|_F^2 = d - \text{tr}(\mathbf{Y}^\dagger \mathbf{Y}) = \text{tr}(\mathbf{Z}^\dagger \mathbf{Z})$ . Note that  $\mathbf{X}\mathbf{Y} \in \mathbb{C}^{d \times d}$  is independent of  $\hat{\mathbf{V}} \in \mathbb{C}^{M \times d}$ , since  $\mathbf{X}\mathbf{Y}$  is a projection to a lower dimension space. Also, the factors  $\mathbf{X}$  and  $\mathbf{Y}$  are independent, since  $\mathbf{X}$  represents the basis of  $\hat{\mathbf{V}}^\dagger \mathbf{V}$  and the basis are not unique. Using similar facts, the matrices  $\mathbf{S}$  and  $\mathbf{Z}$  are also independent. For more details, visit [25].

### B. Proof of Lemma 5

*Proof:* In literature, it is known that the rate loss is upper bounded by the interference terms [25], [51]. Thus, the rate loss bound can be expressed as

$$\Delta R_k \leq \log_2 \left| \mathbf{I}_d + \frac{P}{d\sigma_{ID}^2} \sum_{j \neq k} \mathbb{E} \mathbf{H}_{kj}^\dagger \hat{\mathbf{V}}_j \hat{\mathbf{V}}_j^\dagger \mathbf{H}_{kj} \right|, \quad (53)$$

where  $\mathbf{H}_{kj}^\dagger = \mathbf{U}_k^\dagger \mathbf{H}_{kj}$ . Using Lemma 2, we can write

$$\mathbf{H}_{kj}^\dagger \hat{\mathbf{V}}_j = \mathbf{H}_{kj}^\dagger \mathbf{V}_j \mathbf{X}_j \mathbf{Y}_j + \mathbf{H}_{kj}^\dagger \mathbf{S}_j \mathbf{Z}_j \quad (54)$$

$$= \mathbf{H}_{kj}^\dagger \mathbf{S}_j \mathbf{Z}_j \quad (55)$$

where  $\mathbf{H}_{kj}^\dagger \mathbf{V}_j = 0$  for interference alignment. To make  $\mathbf{H}_{kj}$  orthonormal, let  $\tilde{\mathbf{H}}_{kj} = \mathbf{H}_{kj} \mathbf{W}_{kj} \Lambda_{kj}^{-1/2}$  such that,  $\tilde{\mathbf{H}}_{kj}^\dagger \tilde{\mathbf{H}}_{kj} = \mathbf{I}_d$ , where  $\mathbf{H}_{kj}^\dagger \mathbf{H}_{kj} = \mathbf{W}_{kj} \Lambda_{kj} \mathbf{W}_{kj}^\dagger$  be the eigenvalue decomposition. The above decomposition is similar to SVD,  $\mathbf{H}_{kj} = \tilde{\mathbf{H}}_{kj} \Lambda_{kj}^{1/2} \mathbf{W}_{kj}^\dagger$ , where  $\tilde{\mathbf{H}}_{kj}, \mathbf{W}_{kj}, \Lambda_{kj}$  are

independent of each other. Since  $\mathbf{S}_j$  and  $\mathbf{Z}_j$  are independent as well, the following product can be simplified as

$$\mathbb{E}\mathbf{H}_{kj}^\dagger \mathbf{S}_j \mathbf{Z}_j \mathbf{Z}_j^\dagger \mathbf{S}_j^\dagger \mathbf{H}_{kj} \quad (56)$$

$$\stackrel{(a)}{=} \mathbb{E}\mathbf{W}_{kj} (\mathbf{\Lambda}_{kj}^{1/2})^\dagger \tilde{\mathbf{H}}_{kj}^\dagger \mathbf{S}_j \mathbf{Z}_j \mathbf{Z}_j^\dagger \mathbf{S}_j^\dagger \tilde{\mathbf{H}}_{kj} \mathbf{\Lambda}_{kj}^{1/2} \mathbf{W}_{kj}^\dagger \quad (57)$$

$$\stackrel{(b)}{=} \mathbb{E}\mathbf{W}_{kj} (\mathbf{\Lambda}_{kj}^{1/2})^\dagger \tilde{\mathbf{H}}_{kj}^\dagger \mathbf{S}_j \left[ \mathbb{E}\mathbf{Z}_j \mathbf{Z}_j^\dagger \right] \mathbf{S}_j^\dagger \tilde{\mathbf{H}}_{kj} \mathbf{\Lambda}_{kj}^{1/2} \mathbf{W}_{kj}^\dagger \quad (58)$$

$$\stackrel{(c)}{=} \frac{z}{d} \mathbb{E}\mathbf{W}_{kj} (\mathbf{\Lambda}_{kj}^{1/2})^\dagger \left[ \mathbb{E}\tilde{\mathbf{H}}_{kj}^\dagger \mathbf{S}_j \mathbf{S}_j^\dagger \tilde{\mathbf{H}}_{kj} \right] \mathbf{\Lambda}_{kj}^{1/2} \mathbf{W}_{kj}^\dagger \quad (59)$$

$$= \frac{z}{d} \frac{d}{M-d} \mathbb{E}\mathbf{W}_{kj} \mathbf{\Lambda}_{kj} \mathbf{W}_{kj}^\dagger \quad (60)$$

$$= \frac{z}{M-d} \mathbb{E}\mathbf{H}_{kj}^\dagger \mathbf{H}_{kj} = \frac{z}{M-d} \bar{\Lambda}_{kj} = \frac{zM\mathbf{I}_d}{M-d} \quad (61)$$

where in (a), the decomposition of  $\mathbf{H}_{kj} = \tilde{\mathbf{H}}_{kj} \mathbf{\Lambda}_{kj}^{1/2} \mathbf{W}_{kj}^\dagger$  has been substituted; in (b), the expectation on  $\mathbf{Z}_j$  is carried out, which is approximated to be  $\frac{1}{d} \mathbb{E} \text{tr}(\mathbf{Z}_j \mathbf{Z}_j^\dagger) = \frac{z_j}{d}$  as [25, App. B], where  $z_j$  is the expected chordal distance; in (c), the quantity  $\tilde{\mathbf{H}}_{kj}^\dagger \mathbf{S}_j$  is matrix Beta distributed  $BETA(d, M-2d)$ , which has mean of  $\frac{d}{M-d}$ ; and we write  $\bar{\Lambda}_{kj} = \mathbb{E}\mathbf{H}_{kj}^\dagger \mathbf{H}_{kj} = \mathbb{E}_{\mathbf{H}} \mathbf{U}_k^\dagger \mathbf{H}_{kj} \mathbf{H}_{kj}^\dagger \mathbf{U}_k \leq \mathbf{U}_k^\dagger \mathbb{E}_{\mathbf{H}} \mathbf{H}_{kj} \mathbf{H}_{kj}^\dagger \mathbf{U}_k = M \mathbf{U}_k^\dagger \mathbf{U}_k = M \mathbf{I}_d$ , where the inequality occurs since  $\mathbf{U}_k$  and  $\mathbf{H}_{kj}$  are dependent. Thus, the rate loss bound expression can be given as

$$\Delta R_k < \log_2 \left| \mathbf{I}_d + \frac{P}{d\sigma_{ID}^2} \sum_{j \neq k} \frac{z_j M \mathbf{I}_d}{M-d} \right| \quad (62)$$

$$= d \log_2 \left( 1 + \frac{P}{\sigma_{ID}^2} \frac{M}{d(M-d)} \sum_{j \neq k} z_j \right). \quad (63)$$

### C. Proof of Lemma 7

*Proof:* The inequality in the upper bound comes from (14) as  $\frac{1}{d} \sum_{i=1}^d \|\mathbf{H}_j \mathbf{V}_j^{BAL}\|_F^2 \leq \frac{1}{d} \sum_{i=1}^d \lambda_{ji} \leq \lambda_{j1}, \forall j$ , where the equality occurs when  $z_j = z_j^{EH}, \forall j$ , and the second inequality is due to the fact that the average of  $d$ -values is less than the maximum of them.

The inequality of the lower bound can be derived from the CD decomposition, where the equality occurs, when  $z_j = 0, \forall j$ . For the proposed balanced precoder with the optimum values of  $\mathbf{X}_j^*, \mathbf{Y}_j^*, \mathbf{S}_j^*$  and  $\mathbf{Z}_j^*$ , we can write

$$\begin{aligned} & \|\mathbf{H}_j \mathbf{V}_j^{BAL}\|_F^2 \\ &= \|\mathbf{H}_j \mathbf{V}_j \mathbf{X}_j^* \mathbf{Y}_j^* + \mathbf{H}_j \mathbf{V}_j^{\text{null}} \mathbf{S}_j^* \mathbf{Z}_j^*\|_F^2 \\ &\stackrel{(a)}{\geq} \left\| \mathbf{H}_j \mathbf{V}_j \mathbf{X}_j^* \sqrt{1 - \frac{z_j}{d}} + \mathbf{H}_j \mathbf{V}_j^{\text{null}} \mathbf{S}_j^* \sqrt{\frac{z_j}{d}} \right\|_F^2 \\ &\stackrel{(b)}{\geq} \|\mathbf{H}_j \mathbf{V}_j \mathbf{X}_j^*\|_F^2 \left(1 - \frac{z_j}{d}\right) + \|\mathbf{H}_j \mathbf{V}_j^{\text{null}} \mathbf{S}_j^*\|_F^2 \left(\frac{z_j}{d}\right) \\ &\stackrel{(c)}{\geq} \|\mathbf{H}_j \mathbf{V}_j\|_F^2 \left(1 - \frac{z_j}{d}\right) + \|\mathbf{H}_j \mathbf{V}_j^{\text{null}}\|_F^2 \left(\frac{z_j}{d}\right), \end{aligned}$$

where in (a), the maximum value of norm is upper bounded by trivial selection  $\mathbf{Z}_j = \mathbf{I}_d \sqrt{1 - \frac{z_j}{d}}$ ; in (b), we employ the fact that the trace value in the above norm-expansion is

non-negative for the proposed scheme, as mentioned in the proposition 6; and in (c), the specific  $d$ -dimensional null space  $(\mathbf{V}_j^{\text{null}} \mathbf{S}_j^*)$  can be replaced with any other  $d$ -dimensional null space  $\mathbf{V}_j^n = \mathbf{V}_j^{\text{null}} \mathbf{S}_j^* \in \mathcal{G}_{M,d}$  of  $\mathbf{V}_j$ . ■

### REFERENCES

- [1] N. Zhao, F. R. Yu, and V. C. M. Leung, "Wireless energy harvesting in interference alignment networks," *IEEE Communications Magazine*, vol. 53, no. 6, pp. 72–78, 2015.
- [2] Z. G. Wan, Y. K. Tan, and C. Yuen, "Review on energy harvesting and energy management for sustainable wireless sensor networks," in *IEEE 13th International Conference on Communication Technology*, Sep. 2011, pp. 362–367.
- [3] R. Prasad, S. Devasenapathy, V. Rao, and J. Vazifehdan, "Reincarnation in the ambiance: Devices and networks with energy harvesting," *IEEE Communications Surveys and Tutorials*, vol. 16, no. 1, pp. 195–213, 2014.
- [4] C. Valenta and G. Durgin, "Harvesting wireless power: Survey of energy-harvester conversion efficiency in far-field, wireless power transfer systems," *IEEE Microwave Magazine*, vol. 15, no. 4, pp. 108–120, 2014.
- [5] R. Vyas, B. Cook, Y. Kawahara, and M. Tentzeris, "E-WEHP: A battery-less embedded sensor-platform wirelessly powered from ambient digital-TV signals," *IEEE Transactions on Microwave Theory and Techniques*, vol. 61, no. 6, pp. 2491–2505, 2013.
- [6] I. Krikidis, S. Timotheou, S. Nikolaou, G. Zheng, D. Ng, and R. Schober, "Simultaneous wireless information and power transfer in modern communication systems," *IEEE Communications Magazine*, vol. 52, no. 11, pp. 104–110, 2014.
- [7] M. Khandaker and K.-K. Wong, "Swipt in MISO multicasting systems," *IEEE Wireless Communications Letters*, vol. 3, no. 3, pp. 277–280, 2014.
- [8] Q. Shi, L. Liu, W. Xu, and R. Zhang, "Joint transmit beamforming and receive power splitting for MISO SWIPT systems," *IEEE Transactions on Wireless Communications*, vol. 13, no. 6, pp. 3269–3280, 2014.
- [9] Q. Shi, W. Xu, T.-H. Chang, Y. Wang, and E. Song, "Joint beamforming and power splitting for MISO interference channel with SWIPT: An SOCP relaxation and decentralized algorithm," *IEEE Transactions on Signal Processing*, vol. 62, no. 23, pp. 6194–6208, 2014.
- [10] B. Xu, Y. Zhu, and R. Zhang, "Optimal power allocation for a two-link interference channel with SWIPT," in *Sixth International Conference on Wireless Communications and Signal Processing (WCSP)*, Oct 2014, pp. 1–5.
- [11] Z. Zong, H. Feng, F. Yu, N. Zhao, T. Yang, and B. Hu, "Optimal transceiver design for SWIPT in K-user MIMO interference channels," *IEEE Transactions on Wireless Communications*, vol. 15, no. 1, pp. 430–445, 2016.
- [12] N. Zhao, F. Cheng, F. R. Yu, J. Tang, Y. Chen, G. Gui, and H. Sari, "Caching uav assisted secure transmission in hyper-dense networks based on interference alignment," *IEEE Transactions on Communications*, vol. 66, no. 5, pp. 2281–2294, 2018.
- [13] L. R. Varshney, "Transporting information and energy simultaneously," in *IEEE International Symposium on Information Theory*, July 2008, pp. 1612–1616.
- [14] P. Grover and A. Sahai, "Shannon meets Tesla: Wireless information and power transfer," in *IEEE International Symposium on Information Theory*, June 2010, pp. 2363–2367.
- [15] R. Zhang and C. Ho, "MIMO broadcasting for simultaneous wireless information and power transfer," *IEEE Transactions on Wireless Communications*, vol. 12, no. 5, pp. 1989–2001, 2013.
- [16] L. Liu, R. Zhang, and K.-C. Chua, "Wireless information and power transfer: A dynamic power splitting approach," *IEEE Transactions on Communications*, vol. 61, no. 9, pp. 3990–4001, 2013.
- [17] X. Chen, C. Yuen, and Z. Zhang, "Wireless energy and information transfer tradeoff for limited-feedback multiantenna systems with energy beamforming," *IEEE Transactions on Vehicular Technology*, vol. 63, no. 1, pp. 407–412, 2014.
- [18] V. Cadambe and S. Jafar, "Interference alignment and degrees of freedom of the K-user interference channel," *IEEE Transactions on Information Theory*, vol. 54, no. 8, pp. 3425–3441, 2008.
- [19] N. Garg and G. Sharma, "Sum rate of k-user mimo interference channel for finite constellation inputs with interference alignment," in *National Conference on Communication (NCC)*, March 2016, pp. 1–4.
- [20] T. Xu and X.-g. Xia, "A diversity analysis for distributed interference alignment using the max-SINR algorithm," *IEEE Transactions on Information Theory*, vol. 60, no. 3, pp. 1857–1868, 2014.



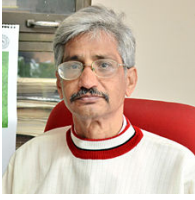
- [21] S. M. Razavi and T. Ratnarajah, "Adaptive LS and MMSE-Based Beamformer Design for Multiuser MIMO Interference Channels," *IEEE Transactions on Vehicular Technology*, vol. 65, no. 1, pp. 132–144, Jan 2016.
- [22] N. Garg and G. Sharma, "Interference alignment in cellular system with multiple d2d networks," in *International Conference on Signal Processing and Communications (SPCOM)*, June 2016, pp. 1–4.
- [23] S. W. Peters and R. W. Heath Jr., "Interference alignment via alternating minimization," in *IEEE International Conference on Acoustics, Speech and Signal Processing (ICASSP)*, 2009, pp. 2445–2448.
- [24] K. Anand, E. Gunawan, and Y. Guan, "Beamformer design for the MIMO interference channels under limited channel feedback," *IEEE Transactions on Communications*, vol. 61, no. 8, pp. 3246–3258, 2013.
- [25] N. Ravindran and N. Jindal, "Limited feedback-based block diagonalization for the MIMO broadcast channel," *IEEE Journal on Selected Areas in Communications*, vol. 26, no. 8, pp. 1473–1482, 2008.
- [26] N. Jindal, "MIMO broadcast channels with finite-rate feedback," *IEEE Transactions on Information Theory*, vol. 52, no. 11, pp. 5045–5060, 2006.
- [27] R. Krishnamachari and M. Varanasi, "Interference alignment under limited feedback for MIMO interference channels," *IEEE Transactions on Signal Processing*, vol. 61, no. 99, pp. 3908–3917, 2013.
- [28] N. Garg and G. Sharma, "Analog precoder feedback schemes with interference alignment," *IEEE Transactions on Wireless Communications*, vol. 17, no. 8, pp. 5382–5396, Aug 2018.
- [29] —, "Precoder quantization for interference alignment with limited feedback," in *IEEE Wireless Communications & Networking Conference (WCNC)*, 2015, pp. 281–286.
- [30] N. Garg and G. Sharma, "A quantization method for precoder feedback in interference channel," in *International Conference on Signal Processing and Communications (SPCOM)*, June 2016, pp. 1–5.
- [31] X. Chen and C. Yuen, "Performance analysis and optimization for interference alignment over MIMO interference channels with limited feedback," *IEEE Transactions on Signal Processing*, vol. 62, no. 7, pp. 1785–1795, 2014.
- [32] J. Park and B. Clerckx, "Transmission strategies for joint wireless information and energy transfer in a two-user mimo interference channel," in *IEEE International Conference on Communications Workshops (ICC)*, June 2013, pp. 591–595.
- [33] S. Lee, L. Liu, and R. Zhang, "Collaborative wireless energy and information transfer in interference channel," *IEEE Transactions on Wireless Communications*, vol. 14, no. 1, pp. 545–557, Jan 2015.
- [34] S. Timotheou, I. Krikidis, and B. Ottersten, "MISO interference channel with QoS and RF energy harvesting constraints," in *IEEE International Conference on Communications (ICC)*, June 2013, pp. 4191–4196.
- [35] N. Zhao, F. R. Yu, and H. Sun, "Adaptive energy-efficient power allocation in green interference-alignment-based wireless networks," *IEEE Transactions on Vehicular Technology*, vol. 64, no. 9, pp. 4268–4281, 2015.
- [36] X. Li, Y. Sun, F. R. Yu, and N. Zhao, "Antenna selection and power splitting for simultaneous wireless information and power transfer in interference alignment networks," in *2014 IEEE Global Communications Conference*, 2014, pp. 2667–2672.
- [37] N. Zhao, F. R. Yu, and V. C. M. Leung, "Opportunistic communications in interference alignment networks with wireless power transfer," *IEEE Wireless Communications*, vol. 22, no. 1, pp. 88–95, 2015.
- [38] —, "Simultaneous wireless information and power transfer in interference alignment networks," in *2014 International Wireless Communications and Mobile Computing Conference (IWCMC)*, 2014, pp. 7–11.
- [39] R. Gupta, A. K. Chaturvedi, and R. Budhiraja, "Improved rate-energy tradeoff for energy harvesting interference alignment networks," *IEEE Wireless Communications Letters*, vol. 6, no. 3, pp. 410–413, 2017.
- [40] C. Yetis, T. Gou, S. Jafar, and A. Kayran, "On feasibility of interference alignment in MIMO interference networks," *IEEE Transactions on Signal Processing*, vol. 58, no. 9, pp. 4771–4782, 2010.
- [41] Ó. González, C. Beltrán, and I. Santamaría, "A feasibility test for linear interference alignment in MIMO channels with constant coefficients," *IEEE Transactions on Information Theory*, vol. 60, no. 3, pp. 1840–1856, 2014.
- [42] C. Wang, T. Gou, and S. a. Jafar, "Subspace alignment chains and the degrees of freedom of the three-user MIMO interference channel," *IEEE Transactions on Information Theory*, vol. 60, no. 5, pp. 2432–2479, 2014.
- [43] N. Garg and G. Sharma, "Precoder quantization vs channel quantization in interference channel with limited feedback," in *National Conference on Communications (NCC)*, March 2017, pp. 1–4.
- [44] G. Bresler, D. Cartwright, and D. Tse, "Settling the feasibility of interference alignment for the MIMO interference channel: the symmetric square case," *IEEE Transactions on Information Theory*, pp. 1–13, 2011.
- [45] —, "Feasibility of interference alignment for the MIMO interference channel," *IEEE Transactions on Information Theory*, vol. 60, no. 9, pp. 5573–5586, 2014.
- [46] M. Razaviyayn, G. Lyubeznik, and Z.-Q. Luo, "On the degrees of freedom achievable through interference alignment in a MIMO interference channel," *IEEE Transactions on Signal Processing*, vol. 60, no. 2, pp. 812–821, 2012.
- [47] N. Garg, A. K. Jagannatham, G. Sharma, and T. Ratnarajah, "Precoder feedback schemes for robust interference alignment with bounded csi uncertainty," *IEEE Transactions on Signal and Information Processing over Networks*, vol. 6, pp. 407–425, 2020.
- [48] N. Garg, J. Zhang, and T. Ratnarajah, "Rate-energy balanced precoding design for swipt based two-way relay systems," *IEEE Journal of Selected Topics in Signal Processing*, pp. 1–1, 2021.
- [49] N. Zhao, F. Yu, and V. Leung, "Wireless energy harvesting in interference alignment networks," *IEEE Communications Magazine*, vol. 53, no. 6, pp. 72–78, 2015.
- [50] Y. Li, L. Zhang, L. J. Cimini, and H. Zhang, "Statistical analysis of mimo beamforming with co-channel unequal-power mimo interferers under path-loss and rayleigh fading," *IEEE Transactions on Signal Processing*, vol. 59, no. 8, pp. 3738–3748, 2011.
- [51] O. E. Ayach and R. W. Heath, "Interference alignment with analog channel state feedback," *IEEE Transactions on Wireless Communications*, vol. 11, no. 2, pp. 626–636, 2012.
- [52] J. Kang, I. Kim, and D. I. Kim, "Wireless information and power transfer: Rate-energy tradeoff for nonlinear energy harvesting," *IEEE Transactions on Wireless Communications*, vol. 17, no. 3, pp. 1966–1981, 2018.
- [53] X. Zhou, R. Zhang, and C. K. Ho, "Wireless information and power transfer: Architecture design and rate-energy tradeoff," *IEEE Transactions on Communications*, vol. 61, no. 11, pp. 4754–4767, 2013.



Navneet Garg received the B.Tech. degree in electronics and communication engineering from College of Science & Engineering, Jhansi, India, in 2010, and the M.Tech. degree in digital communications from ABV-Indian Institute of Information Technology and Management, Gwalior, in 2012. He has completed the Ph.D. degree in June 2018 from the department of electrical engineering at the Indian Institute of Technology Kanpur, India. From July 2018-Jan 2019, he visited The University of Edinburgh, UK. From February 2019-2020, he is employed as a research associate in Heriot-Watt university, Edinburgh, UK. Since February 2020, he is working as a research associate in The University of Edinburgh, UK. His main research interests include wireless communications, signal processing, optimization, and machine learning.



Avinash Rudraksh received B.Tech degree in Electronics & Telecommunication from National Institute of Technology Raipur, India, in 2012 and M.Tech in Signal Processing and Wireless Networks from Institute of Information Technology Kanpur, India, in 2018. He is currently working as a software developer. His research interests include wireless communications and signal processing.



**Govind Sharma** received the B.Tech. and M.Tech. degrees in Department of Electrical Engineering from Indian Institute of Technology Kanpur, India, in 1979 and 1981, and the Ph.D. degree from University of Southern California (USC), in 1984. Since then, he has been a Professor with Department of Electrical Engineering at Indian Institute of Technology Kanpur, India. His general interests span the areas of signal processing and communications, detection and estimation theory, etc.



**Tharmalingam Ratnarajah** is currently with the Institute for Digital Communications, the University of Edinburgh, Edinburgh, UK, as a Professor in Digital Communications and Signal Processing. He was a Head of the Institute for Digital Communications during 2016-2018. His research interests include signal processing and information theoretic aspects of beyond 5G wireless networks, full-duplex radio, mmWave communications, random matrices theory, interference alignment, statistical and array signal processing and quantum information theory. He has published over 400 publications in these areas and holds four U.S. patents. He has supervised 16 PhD students and 21 post-doctoral research fellows and raised \$11+ million USD of research funding. He was the coordinator of the EU projects ADEL (3.7M €) in the area of licensed shared access for 5G wireless networks, HARP (4.6M €) in the area of highly distributed MIMO, as well as EU Future and Emerging Technologies projects HIATUS (3.6M €) in the area of interference alignment and CROWN (3.4M €) in the area of cognitive radio networks. Dr Ratnarajah was an associate editor IEEE Transactions on Signal Processing, 2015-2017 and Technical co-chair, The 17th IEEE International workshop on Signal Processing advances in Wireless Communications, Edinburgh, UK, 3-6, July 2016. Dr Ratnarajah is a Fellow of Higher Education Academy (FHEA).